Cape Peninsula
University of Technology

COST-EFFECTIVE TESTING TECHNIQUES TO CHARACTERISE UHF ANTENNAS

by

CASEY JAMES NIELS MONDE BRYANT

Dissertation submitted in fulfilment of the requirements for the degree:

Masters of Engineering: Satellite Systems & Applications

In the faculty of Engineering and the Built Environment

Department of Electrical, Electronic and Computer Engineering

at the Cape Peninsula University of Technology

Supervisor: Dr. P.G. Wiid

Bellville
September 2022

Declaration

I, Casey James Niels Monde Bryant, declare that the content of this proposal represents my own unaided work, and that the proposal has not previously been submitted for academic examination towards any qualification. Furthermore, it represents my own opinions and not necessarily those of the Cape Peninsula University of Technology.

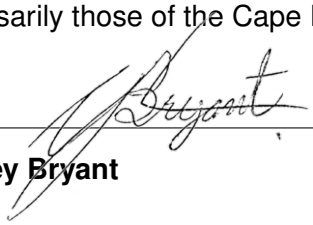

Casey Bryant	**Date**
	26/09/2022

Summary

Engineers require the ability to measure and characterise the reflection coefficient, gain and gain patterns of unknown antennas. Due to the cost of antenna measurement facilities and the associated equipment, many tertiary educational institutes do not have these facilities available. The purpose of this research was to investigate the use of a sports field as a testing range with cost-effective equipment. Measurements were conducted at two commercial ranges and a sports field. The first range was an open area test sight (OATS) where a cost-effective vector network analyser (VNA) (≈R3000) was compared to a commercial VNA (≈R1.5 million). The antennas under test were two identical log-periodic dipole arrays with a frequency range from 180 MHz - 3 GHz. Altair FEKO was used to model the antenna and compare results from different ground plane responses. An anechoic chamber was used to make baseline measurements which were then compared to the FEKO simulation, OATS and sports field measurements. The sports field results had close correlation with the anechoic chamber and OATS measurements. The study finds that by using the two antenna method an antenna can be cost-effectively and reasonably accurately characterised for boresight gain to within 1.7 dB on a sports field. The gain pattern was also achieved on the sports field to within 3 dB of an anechoic chamber measurement. The results enable students and engineers to take antenna measurements at tertiary institutions for under R10,000.

Key-Words: Antenna measurement, Reflection Range, UHF, Gain, Gain Pattern, LPDA, NanoVNA

Dedication

This thesis is dedicated to:
my late father, Jeremy,
my mother, Riette,
my brother, Geoffrey,
and the BTech Lads.

Acknowledgements

I wish to thank:

- Dr. P.G. Wiid for his continuous support, encouragement and teaching, it has been a privilege to have you as my supervisor for this research.
- The South African Radio Astronomy Observatory's Radio Frequency Interference department, with special thanks to Carel van der Merwe, Jason Fynn and Aneshka Bothma. The equipment and helping hands were crucial for this research.
- Fred Thomas for granting me the opportunity to complete the after-hours measurements at the Houwteq Anechoic Chamber.
- My collogues at MESA Solutions for the role each of them played in refining this research.
- Camen Davidowitz for putting up with the late nights, endless weeks and proof reading required to bring this thesis to a tidy conclusion.
- God almighty for his never-ending grace.

The financial assistance of the National Research Foundation (NRF) towards this research is hereby acknowledged. Opinions expressed and conclusions arrived at, are those of the author and are not necessarily attributed to the NRF.

Contents

List of Tables

List of Figures

Abbreviations

AUT	Antenna under test
CAD	Computer aided design
CEM	Computational electromagnetics
CPUT	Cape Peninsula University of Technology
DUT	Device under test
EM	Electromagnetic
EMC	Electromagnetic compatibility
EMF	Electromotive force
EMI	Electromagnetic interference
F'SATI	French South African Institute of Technology
FF	Far field
FSL	Free space loss
GHz	GigaHertz
H	Horizontal
H-Pol	Horizontal polarization
ITU	International Telecommunication Union
ITU-R	International Telecommunication Union Radiocommunication
LPDA	Log-periodic dipole array
MHz	MegaHertz
MoM	Method of moments
OATS	Open area test sight
PEC	Perfect electric conductor
R&S	Rohde & Schwarz
RCA	Reflection coefficient approximation
RF	Radio frequency
SARAO	South African Radio Astronomy Observatory
SOLT	Short-Open-Load-Through
UHF	Ultra high frequency
V-Pol	Vertical polarization
VHF	Very high frequency
VNA	Vector network analyser
VSWR	Voltage standing wave ratio

Variables

σ	Electrical conductivity
ε	Electrical permeability
h	Antenna height
λ	Wavelength
μ	Magnetic permeability
D	Largest antenna dimension
P_r	Power receive
P_t	Power transmit
R	Separation distance
Rx	Receiver
S_{22}	Reflection coefficient on port 2
S_{11}	Reflection coefficient on port 1
S_{12}	Transmission coefficient
S_{21}	Transmission coefficient
Tx	Transmitter

Chapter 1

Introduction

The use of antennas is ubiquitous. Common applications include billions of mobile devices connected to cellular telecommunication towers, aeroplanes communicating with ground stations (as well as other planes) and satellites streaming data to and from the earth. They all have one thing in common: they communicate via radio waves transmitted from specifically designed antennas.

These antennas need to be tested and characterised to ensure they operate as designed. The French South African Institute of Technology (F'SATI) designs and manufactures nano-satellite antennas. To correctly characterise these new antennas, testing is required. An in-house characterisation ability will be more cost-effective as the antenna will be able to undergo physical testing during the design process. This allows early issue detection, in-house performance evaluation, as well as a teaching benefit to students.

Antenna characterisation generally involves an antenna under test (AUT), an antenna with known characteristics, a vector network analyser (VNA) and an antenna test range. Balanis (2016:982) broadly categorises antenna ranges as either outdoor or indoor ranges. This project will focus on outdoor ranges, as they allow for the use of an open area such as a sports field. This reduces costs by making use of already available facilities at tertiary education institutions. The most costly part of antenna measurement is the measurement equipment, costing into the millions of rands. In this study, the author has access to a more cost-effective device, a NanoVNA. This device is compared to renowned test equipment to ensure that such a device can maintain the required level of precision.

1.1 Problem Statement

Although the Cape Peninsula University of Technology (CPUT) actively develops antennas for the nano-satellite market, it currently has no antenna testing facilities of its own. Antenna design is also a research niche of the university, hence, students would benefit from access to a robust testing methodology.

Cost is one of the main factors why the university does not have its own measurement facility. The advanced measurement equipment, space, and material required for a commercial facility can reach millions of rands. However, it is still a requirement to test antennas, and testing at third-party testing facilities is not always viable due to facility access and travel costs. Having a feasible option where students can learn about antenna testing is invaluable.

1.2 Research Objectives

The aim of this research is to study the possibility of using the sports field at CPUT Bellville campus to accurately and cost-effectively characterise an antenna. The specific objectives are as follows:

1. To investigate methods and equipment that could be used to accurately and cost-effectively characterise antennas on a sports field.
2. To determine if a sports field can be characterised sufficiently for use as an antenna characterisation range.
3. To determine to what level of accuracy an unknown antenna can be characterised on a sports field.

The ability to characterise ultra high frequency (UHF) antennas in-house will enable students and engineers to characterise antennas on site. This will remove the need for renting and travelling to third-party test facilities.

1.3 Scope

The scope can be divided into two main types of analysis for this research; analytical modelling in FEKO, and experimental analysis on the sports field. Furthermore, the scope is set out as follows:

1. Test and analyse the NanoVNA compared to a commercial VNA.
2. Write the necessary code to extract the gain from measured or simulated S-Parameter results.
3. Use a computational electromagnetics package to model the AUT and simulate results.
4. Perform at least three sets of the same characterisation measurement to ensure repeatability and accuracy in results.

5. The UHF band ranges from 300 MHz - 3 GHz. This is within the available antenna limits of 200 MHz to 3 GHz, as well as the NanoVNA's defined frequency range.

6. Analyse and compare the gain and gain pattern obtained from different antenna test ranges. Namely, an open area test sight, anechoic chamber and the sports field.

Adhering to the scope and reflecting on the research questions ensured focus throughout the research.

1.4 Thesis Layout

To give the reader background to the current antenna measurement techniques, Chapter 2 provides information on antenna operation and what the gain and gain pattern of an antenna is. Different antenna ranges such as a reflection range and OATS are discussed along with the measurement methods and calculations required to extract gain values from measured data. The methods include the two and three antenna method as well as simulation methods. Measurement equipment such as a vector network analyser (VNA) and the required calibration is also discussed.

Chapter 3 considers the methodology and approach taken to achieve measurements at commercial ranges such as an open area test sight and anechoic chamber. A computational electromagnetics model is drawn in FEKO to run simulations to show expected variations between an OATS and the sports field.

The results between different measurement ranges are compared and discussed in Chapter 4. The final conclusions and recommendations for using a sports field and cost-effective measurement equipment for characterising UHF antennas are given in Chapter 5.

The appendices consist of the Python program used to plot the polar patterns and FEKO 3D polar plots.

Chapter 2

Literature Review and Theory

2.1 Introduction

This review includes antenna operation and characterisation methods as well as the theory behind these methods. The following sections will elaborate on these topics in more detail.

2.2 Principles of Antenna Operation

Antennas are transducers that transmit data through the air via electromagnetic (EM) radiation. EM radiation is brought about by alternating current (ac) signal/s at a specific frequency or range of frequencies which then produces a radiating EM field from the antenna. The propagation from an antenna can be seen in Figure 2.1. The figure, taken from Balanis (2016:2), indicates how the electric field (E-field) travels from the source, through the transmission line into the antenna, where the energy is then able to propagate into free-space as radiation. This propagation is not immediately uniform, creating different field regions around the antenna.

2.2.1 Antenna Field Regions

As the EM radiation leaves an antenna, it requires some distance to form a planar wave front. Balanis (2016:2) subdivides the radiating area around an antenna into three regions: the reactive near-field, the radiating near-field (NF), and the far-field (FF). These regions are not precise and do not abruptly change from one to the other. However, the EM field in each section is different. Figure 2.2 shows an example of these regions, followed by equations to calculate their extent. It is preferable to work in the FF region as this requires less computation and allows for straightforward measurements. Kriel and de Villiers (2020) discusses the NF measurement as being complex. Stating that, in addition to the magnitude of the received power, which is all that is required for FF measurements, both amplitude and phase are also required for the NF measurement. There is also a need for a third antenna which is used as a common reference signal to calculate relative phase between the AUT and measurement antenna.

Foegelle (2002) compares NF and FF, stating that although range length can be reduced by doing NF measurements, they are usually inferior to FF measurements where measurements appear to vary due to mutual coupling between the measurement antenna and AUT. Foegelle further states that FF free-space measurements are uncomplicated to work with, as this is the condition under which all theoretical equations typically used in calculating antenna properties are valid.

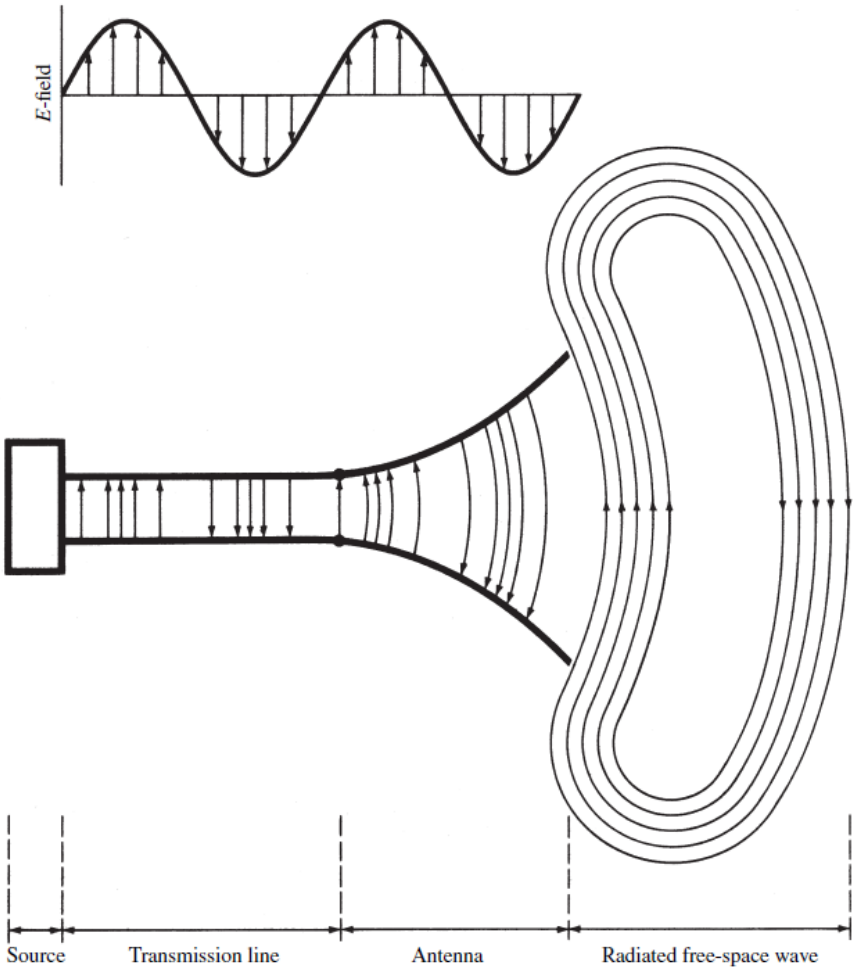

Figure 2.1: E-Field transmission from source to radiated free-space through an antenna (Balanis, 2016:2).

Equation 2.1 refers to the near field distance of an antenna, while Equation 2.2 refers to the minimum radial distance of the far-field region, where D is the maximum antenna diameter in meters and λ is the wavelength in free space of the frequency in question, calculated by $\frac{\text{Speed of light}}{\text{Frequency}}$.

$$\text{Near-field region} < \frac{2D^2}{\lambda} \tag{2.1}$$

$$\text{Far-field region} > \frac{2D^2}{\lambda} \tag{2.2}$$

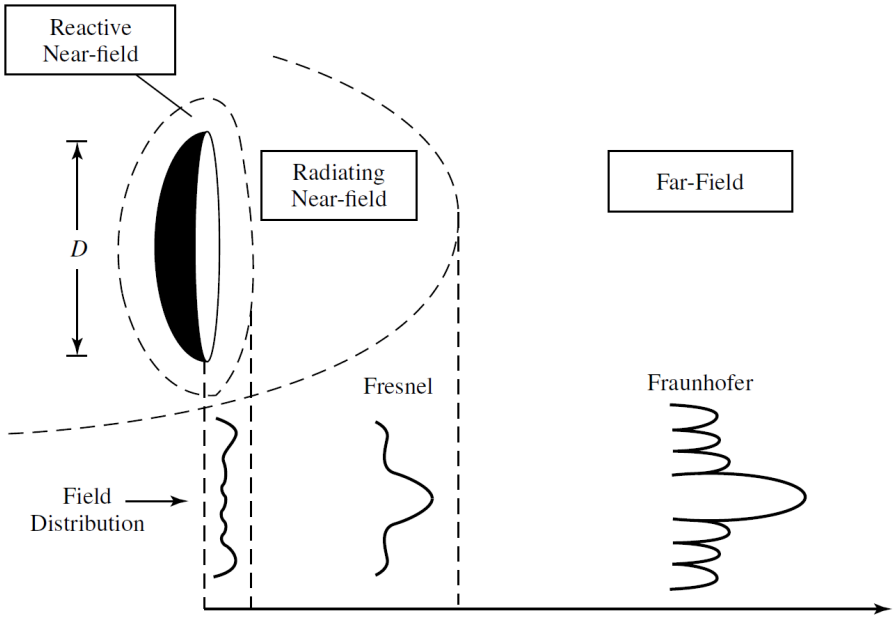

Figure 2.2: Antenna field regions, showing reactive near-field, radiating near-field and far-field (Balanis, 2016:33).

Using Equation 2.2 the far field distance of a half-wave dipole transmitting at 100 MHz can be calculated as:

$$\text{Far-field} = 2\frac{1.5^2}{\left(\frac{3 \times 10^8}{100 \times 10^6}\right)} = 2\frac{1.5^2}{3} = 1.5 \text{ m} \tag{2.3}$$

This shows that a 1.5 m dipole transmitting at 100 MHz (λ = 3 m) will have its far-field starting at 1.5 m from the antenna. Fordham (2016:4) adds that the distance between the source and AUT needs to be sufficiently in the far field to ensure that the wave front approaching the receiving antenna is not overly spherical, as this would produce distortions in AUT side-lobe formation.

Although this section is based on transmitting antennas, all points hold true for a receiving antenna as discussed in the following section.

2.2.2 Reciprocity

Antenna properties, whether transmitting or receiving, are very similar to each other due to the theorem of reciprocity. Connor (1983:4-5) expresses that if a voltage is applied to a circuit X which induces a current in the terminals of circuit Y, then the same voltage applied to circuit Y will induce the same current at the terminals of circuit X, if that circuit is reciprocal. This reciprocity, as stated by Balanis (2016:1001), is the case for most practical antennas. For this reason, tests can be conducted in the transmit or receiving mode for the AUT.

2.3 Characteristics of Interest

When characterising an antenna, there are several specific characteristics of interest as conveyed by Evans (1990:100):

- Gain; the ability of an antenna to direct its power.
- Gain pattern; the different directions in which an antenna radiates.
- Impedance measurements; how much power is reflected instead of radiated by the antenna.

These antenna properties are outlined in more detail below.

2.3.1 Gain

Gain is considered by Balanis (2016:1003) as "the most important figure of merit that describes the performance of a radiator". It is defined as the ratio of the power intensity in a given direction, to the radiation intensity that would be seen if the power were isotropically radiated. This research is focused on realised gain, the gain measurement after mismatch and antenna losses.

Gain could be thought of as how efficiently an antenna radiates its power in a given direction. An isotropic antenna/radiator transmits in a perfect sphere as seen in Figure 2.3 red circle, while a high gain antenna focuses this same power in a certain direction as seen by the blue oval. This means that for the same input power, a high gain antenna will be able to transmit farther in a specific direction, while the isotropic radiator broadcasts a more uniform field. Much like the difference between a light bulb (isotropic radiator) and a torch (high gain antenna).

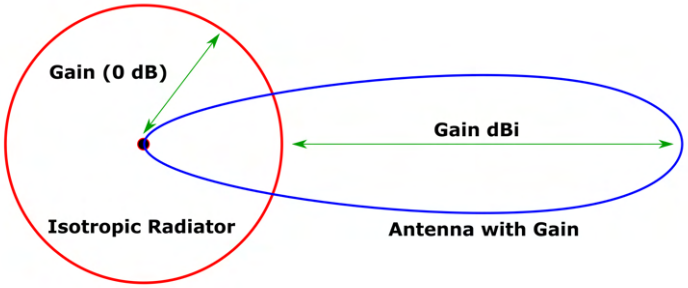

Figure 2.3: Isotropic radiator vs antenna with gain (*What is dBi - Antenna Gain*, 2021).

An isotropic antenna is a theoretical point source, displaying what power would look like if radiated from a point. In the figure above, the antenna with gain is in dBi, the 'i' designates that

it is with respect to an isotropic radiator. There is also dBm (decibels per milliwatt) which is with respect to a milliwatt of power being radiated.

As radiation loses power to the square of distance, it is measured in decibels (dB), a logarithmic unit for expressing the ratio between two quantities. Equation (2.4) explains the decibel power relationship, where power P1 is compared to a reference power P2.

$$Decibel = 10log_{10}\frac{P_1}{P_2} \tag{2.4}$$

This allows measurements that range across several orders of magnitude to be displayed on a more manageable scale. For instance, if the power changes by a factor of 1000, the dB value changes by 30.

2.3.2 Gain Pattern

Connor (1983:2) considers the gain pattern, known also as the polar diagram or radiation pattern, to be the most important property of an antenna. It is the plot of the radiation field strength in different angular directions as shown in Figure 2.4 below.

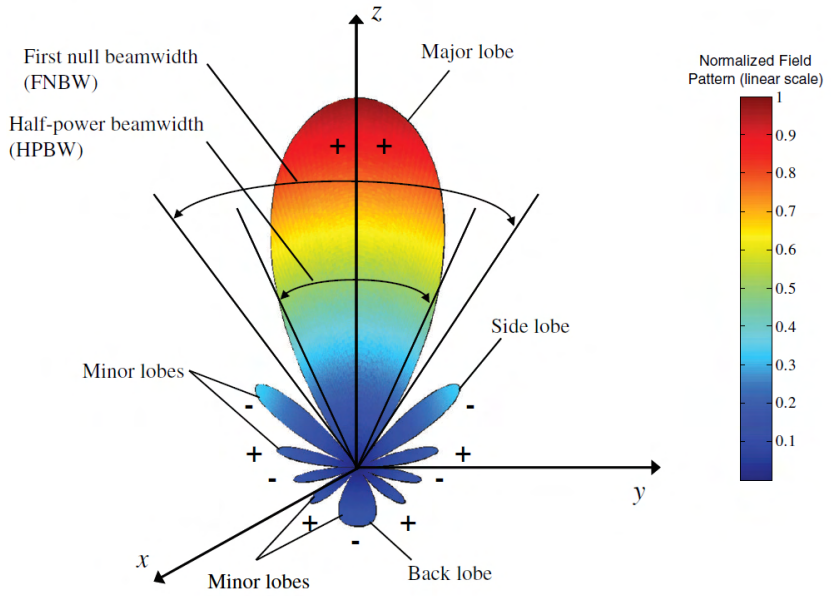

Figure 2.4: Radiation lobes and beamwidths of an antenna gain pattern in polar form (Balanis, 2016:28).

Fordham (2016) discusses the gain pattern as a graphical representation of the radiation distributed by the antenna as a function of direction. It can be plotted in terms of power density, radiation field strength, or decibels and can be absolute or relative to some reference level, often having the peak gain as the reference level. These patterns can be displayed on a rectangular or polar coordinate system as a function of the spherical coordinates.

This section covered the characteristics of interest for an antenna, in the following section, different measurement parameters and equipment for measuring antenna characteristics are covered.

2.4 Characterisation Equipment and Parameters

Balanis (2016:981) notes that with the improvement of special analytical characterisation methods, such as the Finite Element, Moment Method and Finite Difference Time Domain method, the group of antennas that cannot be analytically investigated are rapidly decreasing. However, there are still several complex antenna configurations with discrete excitation methods that have yet to be analytically examined. Furthermore, experimental results are required to validate the analytical methods to ensure real-world applicability. Measurement equipment and the parameters used for experimental characterisation are covered in this section.

2.4.1 Scattering Parameters

Scattering parameters or S-Parameters are widely used in electrical engineering to describe the behaviour of linear, multi-port electrical networks responding to stimulation by electrical signals. These parameters are generally measured using VNAs. Figure 2.5 below shows the S_{11} through S_{22} parameters and how they relate to each other as given in Nyikayaramba and Murmann (2020).

Two S-parameters represent the reflection coefficients at ports 1 and 2 respectively (S_{11} and S_{22}) while the two directions for the transmission coefficients of the ports are represented by S_{12} and S_{21}.

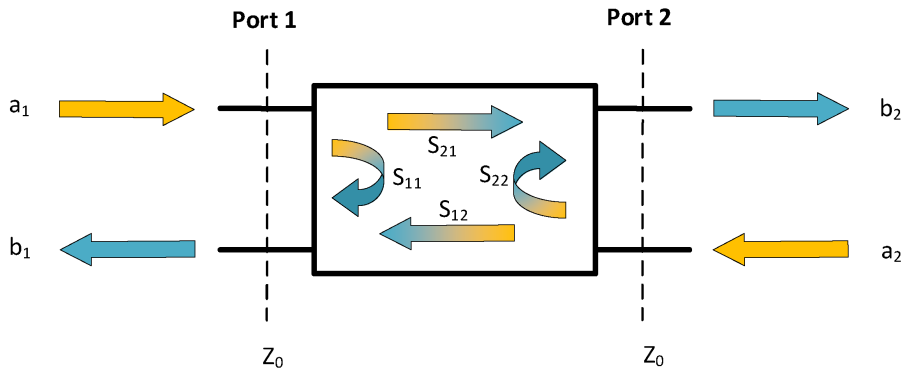

Figure 2.5: S-parameters of two port VNA showing reflection (S_{11}, S_{22}) and transmission (S_{21}, S_{12}) coefficients (Nyikayaramba and Murmann, 2020).

Bevelacqua, P (2015) discusses the reflection coefficient (S_{11}) as the most regularly quoted antenna parameter. This is due to it representing the antenna return loss which informs the

user of how much power is reflected by the antenna at the tested frequency range. A S_{11} value of 0 dB means that all power delivered to the antenna is reflected. The rule of thumb for a good antenna is -10 dB at the frequency of interest.

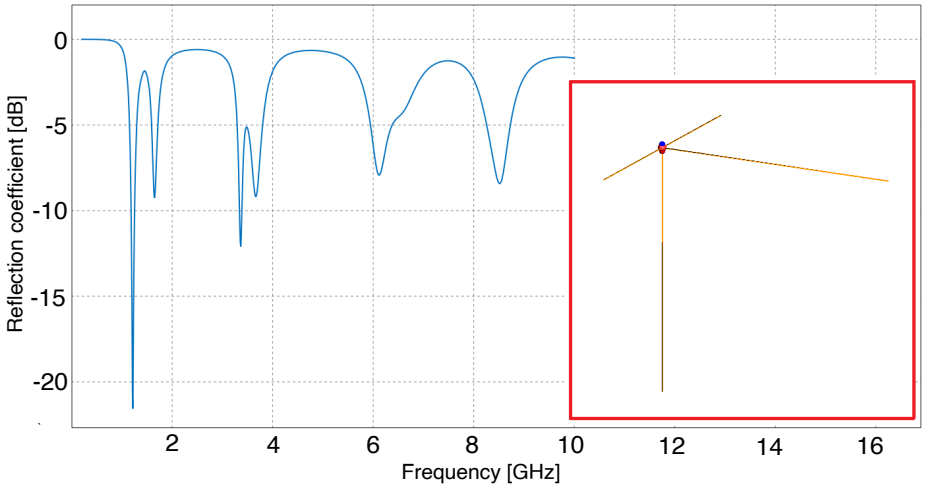

Figure 2.6: Reflection coefficient (S_{11}) of arbitrary antenna as constructed in Altair FEKO (2021). The antenna used for this simulation is displayed in the red box, and is seen to be well matched at 1.2 GHz (-22 dB) and 3.35 GHz (-12 dB).

An antenna made of three perpendicular dipoles of 61.18 mm displayed in Figure 2.6 has a S_{11} response from 200 MHz to 10 GHz as shown. It can be noted that the antenna has two points under -10 dB, at 1.2 GHz (-22 dB) and 3.35 GHz (-12 dB). These points are where the antenna operates most efficiently, and therefore would make a good radiator at those frequencies.

2.4.2 Input Impedance

Impedance measurements are taken to ensure the maximum power transfer from the signal source to the transmitting antenna or from the receiving antenna to the receiver or measurement instrument. This is required as the transmitter impedance is normally resistive (Connor (1983:3)). This means that the antenna should be resistive to be impedance matched, ensuring maximum power transfer between transmitter, feed lines and antenna. Fordham (2016) measures this by measuring the voltage standing wave ratio (VSWR) or reflection coefficient (S_{11}) of the antenna. These two parameters are linked by Equations 2.5 and 2.6.

$$|S_{11}| = \frac{VSWR - 1}{VSWR + 1} \tag{2.5}$$

$$VSWR = \frac{1 + |S_{11}|}{1 - |S_{11}|} \tag{2.6}$$

Ensuring a good impedance match lowers the reflected power and is shown by the reflection

coefficient discussed further in Section 2.4.1. Transmitters and cables for radio frequencies (RF) purposes are usually impedance matched to 50 Ω. This is a compromise between best power transmission at $\approx$30 Ω and ideal signal transmission at $\approx$75 Ω as discussed by Gilmour (1986). Using two matched antennas, transmission can be achieved. The transmission strength can be calculated using Friis transmission equation.

2.4.3 Friis Transmission Equation

A good understanding of Friis free space equation (Friis (1946)) is essential, as it is utilised in most antenna characterisation methods. It should be noted that the equation does not include losses through radiation efficiency or impedance mismatch, etc, and is assumed that the antennas are bore-sighted for maximum transmission directivity.

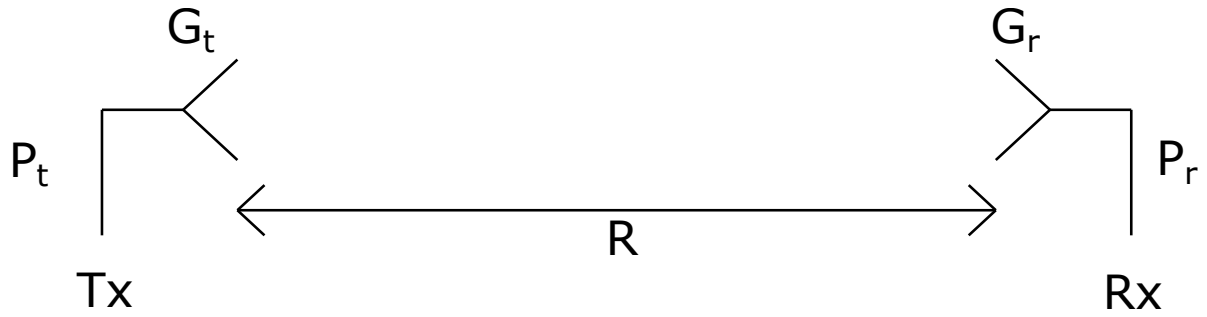

Figure 2.7: Basic two antenna transmission set up.

Figure 2.7 shows two antennas separated by distance R. The left side being the transmit antenna with a transmit power[1] P_t and a gain of G_t while the right receives power P_r with a gain of G_r. These variables are used in Equation 2.7 and 2.8.

$$\mathbf{P_r} = \mathbf{P_t}\left(\frac{\lambda}{\mathbf{4\pi R}}\right)^{\mathbf{2}}\mathbf{G_t G_r} \tag{2.7}$$

$$\mathbf{G_r} = \frac{\mathbf{P_r}(\mathbf{4\pi R})^{\mathbf{2}}}{\mathbf{P_t G_t}\lambda^{\mathbf{2}}} \tag{2.8}$$

Equation 2.7 is the Friis free space transmission formula used to calculate the receive power. Rearranging this gives Equation 2.8 used to calculate the gain of the receive antenna when the transmit power and gain, receive power, wavelength and separation distance are known. These powers are measured most efficiently by using a vector network analyser as it acts as the signal source and receiver.

[1]The t and r subscripts denote transmitter and receiver respectively.

2.4.4 Vector Network Analyser

A Vector Network Analyser is considered by Hiebel (2007) to be the most complex and versatile piece of test equipment that an RF engineer can use. This high-precision, high-cost device is used to measure reflection and transmission of a DUT across a configured frequency range. It does this by transmitting a specific frequency signal and monitors for a return signal at the same frequency. This transmission and receive frequency sweep is done across the selected frequency band. CPUT has a Hewlett Packard VNA as seen in Figure 2.8. The VNA is a large piece of equipment and should be moved with utmost caution to avoid damaging components.

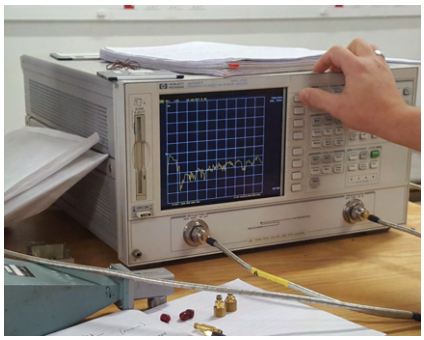

Figure 2.8: HP 8720ET transmission/reflection vector network analyser.

VNAs can be single or multi-port devices with data being saved in a .snp file, known as a Touchstone file. The *n* in the file extension represents the number of ports involved in the measurement. The data contained in a Touchstone file as described by the specification from TechAmerica (2009) is "an ASCII text file used for documenting the n-port network parameter data of an active or passive interconnected network". The data in the file consists of a preamble informing the reader of the type of device and settings used to make the measurement. The pre-amble is then followed by rows consisting of the frequency and the DUT response at each specified frequency. The response is captured in phase and scattering parameter form as discussed in Section (2.4.1).

Measurement accuracy and repeatability are of high importance, however, due to the sensitive signals measured by VNAs, inaccuracies for both phase and amplitude should be expected. There are three main types of errors. Dunsmore (2007) categorises these errors into the following:

Systematic errors

- Due to hardware imperfections, usually predictable.

Drift errors

- Happens after calibration, usually due to temperature change.

Random errors

- Comes from instrument switching/internal noise, usually unpredictable.

By using the VNAs standard defined calibration kit the systematic and drift errors can be minimised by vector-error correction. This is done by means of a short, open, load and through (SOLT) calibration which calibrates the VNA to a reference plane. This allows the VNA to calibrate out the effect of cables or other elements up to the DUT connection ports.

2.4.5 NanoVNA

A large part of this research is based on a cost-effective alternative to commercial VNAs known as the NanoVNA_V2 or S-A-A-2. This low cost VNA was developed by HCXQS (see NanoRFE (2019)) in collaboration with OwOComm (2020) for measurement of antennas, filters, duplexers and amplifiers. It is based on the NanoVNA design by Edy555 (2019).

The NanoVNA V2 boasts a dynamic range of up to 60 dB across a frequency range of 50 kHz - 3 GHz with the NanoVNA V2 Plus 4 boasting more dynamic range and a higher maximum frequency. See Appendix A for full specifications taken from NanoRFE (2019).

2.4.5.1 NanoVNA comparison

John (2021) compared his NanoVNA ($170) to a Keysight FieldFox VNA ($12000) with three different tests: a 900 - 2000 MHz directional coupler, a 980 - 1150 MHz bandpass filter and a 7.6 m length of RG-214 cable. Across the three tests, the largest deviance of the NanoVNA from the FieldFox was 1.4 dB, with majority of tests being accurate to within 1 dB.

Measurement equipment and parameters have been covered in this section. The following section discusses the different types of testing ranges.

2.5 Antenna Ranges

Antenna testing and evaluation are performed in antenna ranges that are broadly categorised as either indoor or outdoor by Balanis (2016:982). Indoor ranges have the advantage of accessibility, irrespective of weather or time of day. However, they are limited by building size and high cost. Outdoor ranges have larger areas and can therefore more easily produce the ideal incident uniform plane wave on the AUT. As calculated in Equation 2.3, the far-field distance of a typical VHF antenna at 100 MHz is 1.5 m, excluding the space behind and around the antenna. This distance increases as frequency increases. As mentioned previously, outdoor ranges will be selected to allow for the use of a sports field as a possible antenna range. This will give a large enough area to allow for mitigation of unwanted reflections. Different types of

ranges are explored in the following section, including a reflection range which is most similar to the sports field.

2.5.1 Anechoic Chamber

The gold standard for antenna ranges are currently anechoic chambers. These chambers simulate free-space by blocking out external interference and absorbing electromagnetic waves inside the chamber, allowing for consistently repeatable results (Balanis (2016:983)). The absorption is achieved by using radar absorbing material seen on the walls in Figure 2.9.

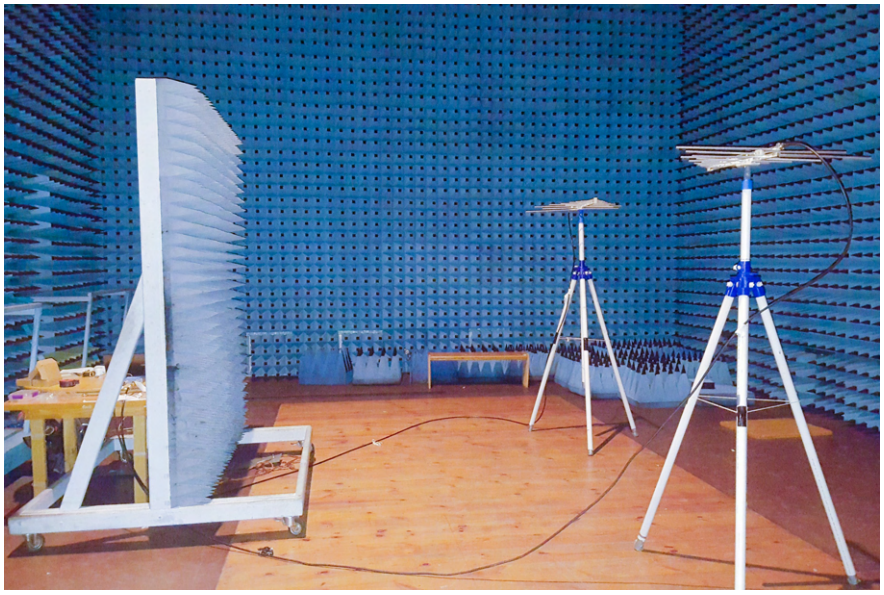

Figure 2.9: Houwteq anechoic chamber. The walls, roof and floor (under the wood shown) are lined with radar absorbing material.

Although these chambers offer superior measurements, their cost can reach into the millions of rands to build, and cost thousands of rands to hire for a day.

2.5.2 Elevated Range

Elevated ranges are designed to operate as free-space ranges over smooth terrain. The antennas are mounted on tall towers, 8 m or higher, built ideally out of non-reflective material. Balanis (2016) states that the source antenna is carefully selected for its directivity and side lobe level. This set up allows minimal reflections, and those that do occur can be reduced by using signal-processing techniques such as modulation tagging.

The disadvantage of this system is the towers that must be built. They must be tall enough as not to see the ground reflections, while being strong enough to withstand deformation due to wind. It is also costly to build and maintain these towers.

2.5.3 Slant Range

The slant range is considered a free-space range with the source antenna placed near the ground, and the AUT and its positioner on top of a tall non-conducting tower (Figure 2.10). The source antenna is positioned to allow maximum pattern directivity toward the test antenna, with the first null directed toward the ground specular reflection point as mentioned in Arnold (1966). This aids in reducing reflections by directing a low-power radiation area in the most likely direction of reflection.

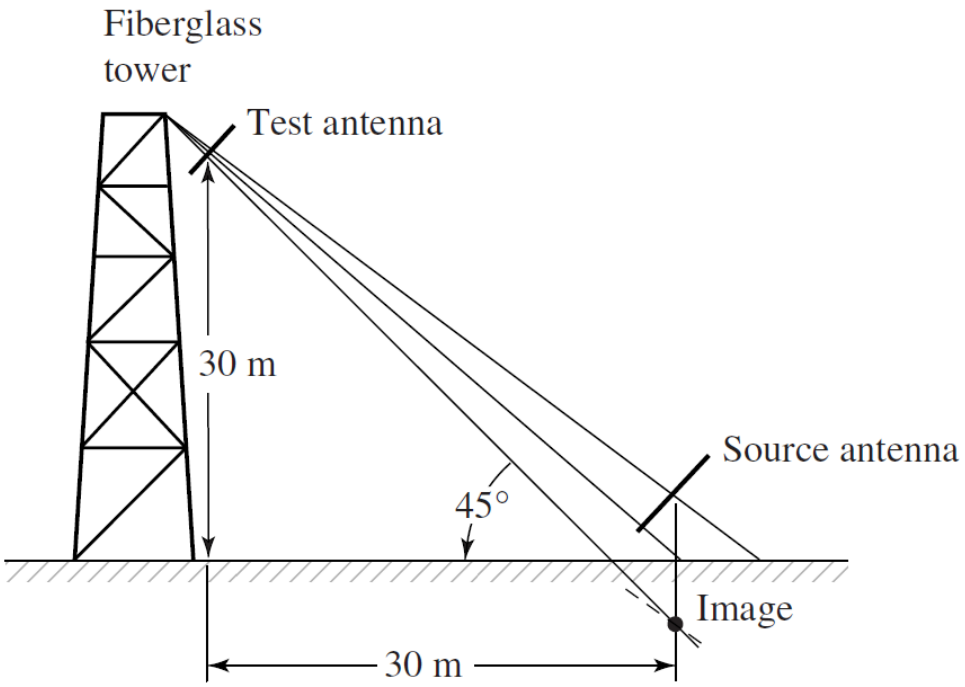

Figure 2.10: Slant range geometries (Balanis, 2016:984).

The slant range has similar disadvantages to the elevated range, in that it needs to be built and maintained for safe operation.

2.5.4 Reflection Range

Hemming and Heaton (1973) discusses the reflection range as being designed to produce constructive interference on the region of the test antenna, which is referred to as the “quiet zone”. It is advised that the illuminating field has a small and symmetrical amplitude taper, which is achieved by adjusting the height of the transmitting antenna. Figure 2.11 displays the geometrical arrangement of a reflection range. Hemming and Heaton (1973) go on to state that reflection ranges are outdoor type ranges and use the ground plane as the reflection surface, making this method suitable for use on a sports field without the need for large towers as required in the elevated and slant ranges.

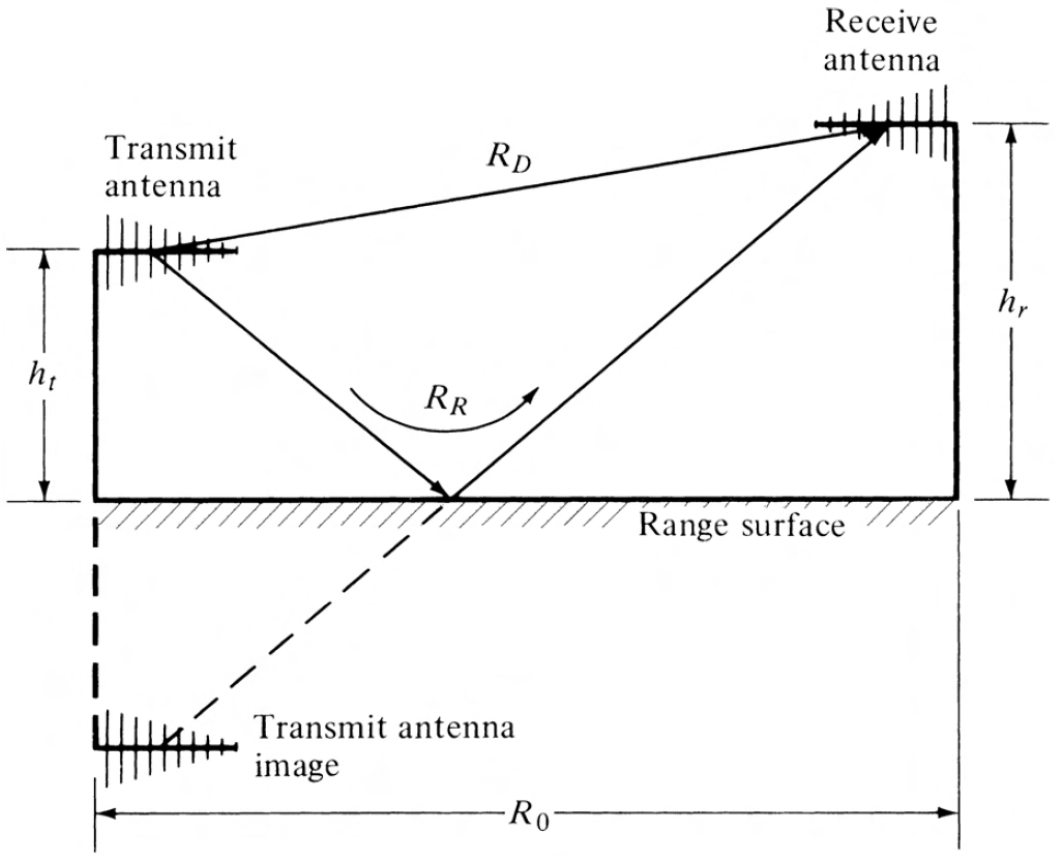

Figure 2.11: Arrangement of a general reflection range (Hemming and Heaton, 1973).

The transmit signal can arrive at the receive antenna through the direct path (R_D) and the reflected path (R_R). This causes the same signal to arrive at the receive antenna with varying phase. Either adding in phase, or out of phase. This can be accounted for mathematically by calculating for the phase difference as outlined in Section 2.6.5. This calculation method is extremely intensive as the antenna height needs to be manipulated for each individual frequency.

To suitably use the ranges covered, specific methods need to be used. These methods, discussed in the next section, have criteria to be met which aid in improving the measurement accuracy.

2.6 Characterisation Methods

There are several methods that can be employed to make realised gain measurements in the far-field. Balanis (2016:1006-1010) mentions the two-antenna method, three-antenna method and ground reflection method. All of which, with others, are discussed below.

2.6.1 S-Parameter Method

Julies (2018) discusses the S-parameter method for determining an unknown antenna's gain and radiation pattern. The S-parameter method focuses on measuring balanced-fed input impedance of antennas by extracting impedance characteristics which are formulated using the complex, frequency dependent S-parameters discussed in Section 2.4.1. Fukasawa et al. (2012) discusses an extended S-parameter method that can be applied to measure the impedance, radiation pattern, efficiency, and coupling between antennas as applied in Yanagi, Fukasawa and Miyashita (2016). This was applied to electrically small antennas, where the antenna size is far smaller than the wavelength.

Most of the methods that follow make use of S-parameters, in particular the S_{21}, as this can be seen as transmission efficiency: power sent versus power received at a specific frequency.

2.6.2 Single Antenna Method

The single antenna method, known also as image theory (Sandrawarman, 2014), is a method where, barring the measurement equipment, only the AUT and a reflector is required. The test antenna is used to transmit, and receive, the signal. With calculations, the gain of the unknown antenna can be found with acceptable accuracy, as demonstrated in both Ameya, Matsukawa and Kurokawa (2018) and Glimm et al. (2000).

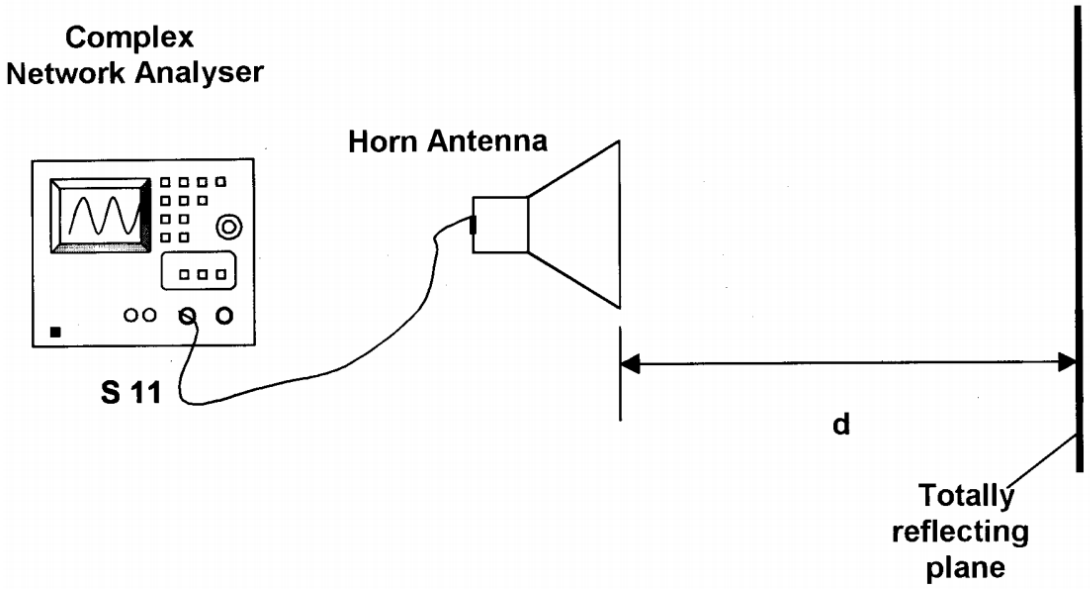

Figure 2.12: Arrangement of one-antenna method as seen in Glimm et al. (2000). The AUT is used as the transmit and receive antenna by bouncing the transmitted signal off a reflecting plane at a known distance.

The key attribute of this method is the simplicity of the setup, which can be seen in Figure 2.12. Glimm et al. (2000) for instance, was able to acquire an unknown antenna's gain employing this

method over a frequency range of 1.1 GHz to 1.7 GHz. Seeing no deviation larger than 0.25 dB compared to the manufacturer's antenna data and theoretical calculations.

2.6.3 Two-Antenna Method

The two-antenna method requires the use of two antennas separated by a distance R which (ideally) satisfies the far field criterion. Balanis notes that the antennas need to be polarisation matched and bore-sighted for maximum directional radiation (Balanis, 2016).

By using the Friis free space transmission Equation (2.7) with two identical antennas allows for $G_{Tx} = G_{Rx} = G$. This simplifies the Friis free space equation to be rewritten as Equation (2.9). Giving the gain of the two identical antennas in decibel. The transmission efficiency ($\frac{P_{Rx}}{P_{Tx}}$) is calculated from the measured transmission coefficient S_{21} (in linear form), wavelength (λ), and separation distance (R) between the two antennas (Mistry et al. (2019) and Julies (2018)).

$$G_{dB} = \frac{1}{2}\underbrace{\left[20log_{10}\left(\frac{4\pi R}{\lambda}\right)\right.}_{FSPL} + \underbrace{\left.20log_{10}(S_{21})\right]}_{S_{21}} \tag{2.9}$$

where

G_{dB} = gain of identical antennas (dB)
R = separation distance (m)
λ = operating wavelength (m)

Equation 2.9 is a combination of two parts, the free space path loss (FSPL) and the S_{21} transmission efficiency part. FSPL is the loss that occurs as the wave propagates through free space, knowing the separation distance *R*, this can be calculated for a given frequency. The S_{21} part is measured by a VNA as discussed in Section 2.4.4.

2.6.4 Three-Antenna Method

When dealing with unknown antennas, the three-antenna method can be used to measure the gain of three unknown antennas, a, b, and c. Balanis (2016:1007) discusses the method by stating that a combination of all three antennas need to be used to make measurements. These measurements should then be calculated by simultaneously solving the following three equations.

Antenna a-b combination:

$$(G_a)_{dB} + (G_b)_{dB} = 20log_{10}\left(\frac{4\pi R}{\lambda}\right) + 10log_{10}\left(\frac{P_{rb}}{P_{ta}}\right) \tag{2.10a}$$

Antenna a-c combination:

$$(G_a)_{dB} + (G_c)_{dB} = 20log_{10}\left(\frac{4\pi R}{\lambda}\right) + 10log_{10}\left(\frac{P_{rc}}{P_{tb}}\right) \tag{2.10b}$$

Antenna b-c combination:

$$(G_b)_{dB} + (G_c)_{dB} = 20log_{10}\left(\frac{4\pi R}{\lambda}\right) + 10log_{10}\left(\frac{P_{rb}}{P_{ta}}\right) \tag{2.10c}$$

Having one known antenna in the measurement cycle allows for a control group to be used to ensure accurate results. This method is rather labour intensive, and would not be suitable to ascertain an antenna pattern.

2.6.5 Ground Reflection Method

Section 2.5.4 discusses the ground reflection range itself while this section will cover the requirements and calculations behind the method. The ground reflection method was discussed by Hemming and Heaton (1973) as early as the 1970s. They proposed that the method could be used to find the absolute gain of wide-beam antennas in the frequency range of 250 to 400 MHz. It was also stated that the accuracy achieved was within 0.27 dB, with a confidence level of 95%.

Balanis (2016) notes this method for use on moderately broad-beam antennas, usually below 1 GHz, with the method considering the specular reflections from the ground plane as seen in Figure 2.11. This method works best with linear antennas in horizontal polarization. Requiring modification for looped and slot radiators.

The first requirements for this method are that the receiving antenna height $h_r \geq 4D$ and that $h_r \geq 4\lambda$.

The formula for finding the gain of an antenna by use of this method, as presented in Balanis (2016) is seen below.

$$(G_a)_{dB} + (G_b)_{dB} = 20log_{10}\Big(\frac{4\pi R_D}{\lambda}\Big) + 10log_{10}\Big(\frac{P_r}{P_t}\Big) - 20log_{10}\Big(\sqrt{D_A D_B} + \frac{rR_D}{R_R}\Big) \quad (2.11)$$

Where:

$(G_a)_{dB}$ & $(G_b)_{dB}$	=	Gain of respective antennas (dB)
P_r	=	Power received (W)
P_t	=	Power transmitted (W)
λ	=	Operating wavelength (m)
D_A & D_B	=	Respective antenna directivity
R_R & R_D	=	Separation lengths for direct and reflected waves (see Figure 2.11)

The factor r is found by adjusting the transmit antenna height so that the field at the receive antenna is minimised. These values are then recorded using a ($'$) prime above the coefficient. After which, the same values are recorded at a maximum receive field. Once the respective values have been determined, they can be input into Equation 2.12 below.

$$r = \left(\frac{R_R R'_R}{R_D R'_D}\right)\left[\frac{\sqrt{(P_r/P'_r)(D'_A D'_B)}R_D - \sqrt{D_A D_B}R'_D}{\sqrt{(P_r/P'_r)}R_R + R'_R}\right] \quad (2.12)$$

The result for *r* is then put into Equation 2.11 which improves the removal of the reflected wave as discussed in Section 2.5.4.

As Equation 2.11 is frequency dependant, a new answer to equation 2.12 will be required for each different frequency. This makes the method extremely time-consuming over a large frequency range and impractical for polar pattern measurements.

2.6.6 Time Domain Method

Time domain reflector measurements, as seen in Koech (2019) and Julies (2018), can be used to find the gain of an unknown antenna. Up to now, most of the methods considered were in the frequency domain, however, Julies (2018) mentions that to accurately characterise an unknown antenna, both frequency and time-domain measurements should be conducted. By using the Inverse Fourier Transform present on some vector network analysers, it is possible to see time on the horizontal axis while the vertical axis displays the signal magnitude. Being in the time domain allows for time domain gating, a method of cleaning up unwanted signal and environmental reflections, as discussed in Chen, Stang and Moghaddam (2016) and Chen and Xiong (2019). An array of other measurement techniques in the time domain with the use of convolution filters are also possible, as seen in Adhyapak, Chen and Shimada (2017), where

the deconvolution filter assists compression of the time-domain pulse to distinguish direct waves from reflected waves.

The methods covered so far have been for experimental measurements, the following section covers analytical techniques to assist antenna characterisation methods.

2.6.7 Analytical Methods

Altair FEKO (2021) is a computational electromagnetics (CEM) software package that uses the Method of Moments (MoM) solver to perform field calculations on arbitrary shaped bodies. This forms a key part of the analytical modelling and simulation of this research. As stated in Phiri (2017:39), the MoM solver is widely used in antenna engineering and is ideal for scattering and radiation or any computational electromagnetic simulation problems.

Simulations will be done to have a model to compare the experimental results to. This will allow for an experimentally proven model to be drawn up which could then be used for simulation testing. Phiri (2017:40) discusses using the default MoM solver in FEKO to produce a full-wave propagation model, involving the modelling of transmit and receive antennas in the presence of an infinite dielectric ground plane. This infinite ground plane should simulate the electrical characteristics of real ground, absorbing and reflecting as might be expected on the sports field.

2.7 Sports Field Characteristics

Most educational institutions have a sports field. This flat, open area holds promise as a cost-effective alternative to a ground reflection range. Figure 2.13 shows the CPUT oval track and sports field, showing that the field is lower than the surrounding ground. This rise out of the field could provide some noise and reflection attenuation as discussed in Phiri (2017:42), regarding the soil berm at Karoo Array Processor Building near the Square Kilometre Array core. The gradient out of the field will also reflect the majority of transmitted radiation into the sky instead of back towards the AUT.

Figure 2.13: CPUT Bellville sports field (image captured on Google Earth).

2.7.1 Modelling Soil Characteristics

Due to the variation in soil characteristics, FEKO does not have set parameters to apply to a soil ground plane. The International Telecommunication Union (2021) (ITU), however, has obtained the required properties of multiple types of ground cover, including water, seawater, vegetation, ice and soil for frequencies up to 1000 GHz. The three required parameters to define a soils characteristics as stated by the ITU are:

- the magnetic permeability, μ
- the electrical permittivity, ε, and
- the electrical conductivity, σ

Soil has a complex relativity that changes with respect to frequency, temperature, soil composition and moisture. This, as was done in the ITU-R P.527-6, can become a study on its own, but is not the focus of this research. Instead, the International Telecommunication Union (2021) will be used similarly to Phiri (2017) where the values were taken from the ITU-R. Figure 2.14 shows the conductivity and permittivity characteristics of wet ground and medium dry ground with respect to frequency.

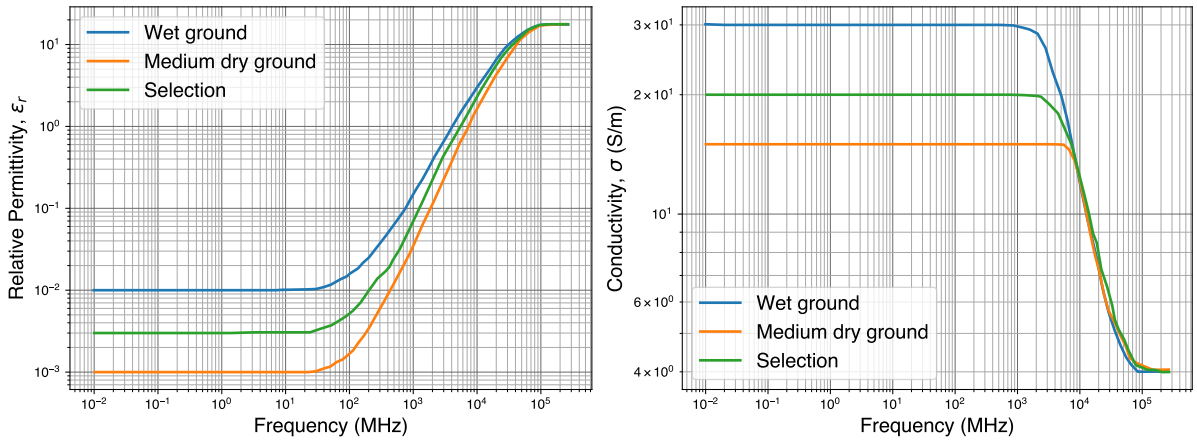

(a) (b)

Figure 2.14: Relative permittivity (a) and conductivity (b) of wet, medium dry and selected (selection) soil with respect to frequency. Adapted from (International Telecommunication Union, 2021)

The third line on the plots, labelled selection, will be used for simulating as the sports field ground does get watered, and therefore, a midpoint will be taken for simulating soil effects.

2.8 Cost of Antenna Measurement

One recurring factor throughout the literature is the initial cost required to set up an antenna measurement facility; with the first being the space required. Either an indoor area for an anechoic chamber, which runs into the millions of rands, or a large open area. However, losing a large area to something as niche as antenna measurements is costly in urban areas. An open area test range also requires maintenance otherwise it will deteriorate within a few years. Once an area has been selected, test equipment is required, and, as mentioned by Ambatali (2018) this equipment is usually too expensive to allow use at classroom level. With the rapid rate of improvements in technology, measurement equipment is becoming cheaper, which could allow accurate measurements to be conducted at a better price point.

2.9 Conclusion

Characterisation techniques such as one, two and three antenna methods, antenna range possibilities and measurement equipment were reviewed in this section. It was found that the two antenna method would be suitable for the required testing as this is an accurate and simple method. The ranges discussed all show promise with the reflection range showing similarities to using the sports field. This will allow a similar setup as discussed in the ground reflection method, however, filtering to remove the reflections will need to be investigated to simplify

for the large frequency range of interest. In the following chapter cost-effective measurement equipment will be used to test two identical, calibrated antennas at dedicated antenna ranges. Using more cost-effective portable equipment will allow possible characterisation of a sports field as a test range.

Chapter 3

Research Methodology

3.1 Introduction

Accurate antenna measurements are a science in their own right. They usually require specialised testing equipment and a dedicated testing facility. The cost for these testing facilities can be so large that tertiary educational institutions do not even consider them. Using a cost-effective measurement solution and commercial measurement equipment, tests were conducted at industry standard facilities. The results from these tests acted as a baseline for measurements taken on the sports field. This comparison allowed for characterisation of the sports field and to quantify to what level of accuracy an unknown antenna can be measured at an easily accessible facility.

3.2 Research Instruments

The available equipment for comparison and their cost estimates are shown in Table 3.1 to inform the reader of the costs associated with these types of devices.

Table 3.1: Key equipment available for antenna measurements with rudimentary information.

Equipment	Description	Type	Owner	Approx. Cost (R)
HP 8720ET	Transmission Reflection, 2-port, 50 MHz - 20 GHz	VNA	CPUT	1.5 million
R&S ZVB8	Rohde & Schwarz, Full 4-port, 300 kHz - 8 GHz	VNA	SARAO	1.5 million
ShockLine ME7868A	Anritsu, Fibre connected, full 2-port, 1 MHz - 43.5 GHz, (demo)	VNA	Anritsu	1 million
NanoVNA V2 Plus4	Transmission reflection, 2-port, 50 kHz - 4.4 GHz	VNA	MESA Solutions	3,500
NanoVNA V2	Transmission reflection, 2-port, 50 kHz - 3.6 GHz	VNA	CPUT	1,200
HP 85052D	Calibration Kit, DC - 26.5 GHz	Calibration	CPUT	90,500
DS-18300	A-INFO LPDA, 180 MHz - 3 GHz, 6 dB gain	Antenna	CPUT	3,800
Coaxial Cable	N-Type male cables, 2 x 5 m	Cables	CPUT	6,000

With replacement costs this high, the devices are rightfully locked away in laboratories, only to be operated under supervision. This means students seldom get to experiment with the equipment, and as such rarely become comfortable with operating them. In 2021, however, several NanoVNAs were purchased by CPUT's electrical engineering department. Due to the low cost of these devices, students could use them. This allowed the author to test the device and compare it to the commercial VNAs seen in Table 3.1. Initial lab results between the cost-effective NanoVNA and CPUT's commercial HP 8720ET are seen in Figure 3.1 below.

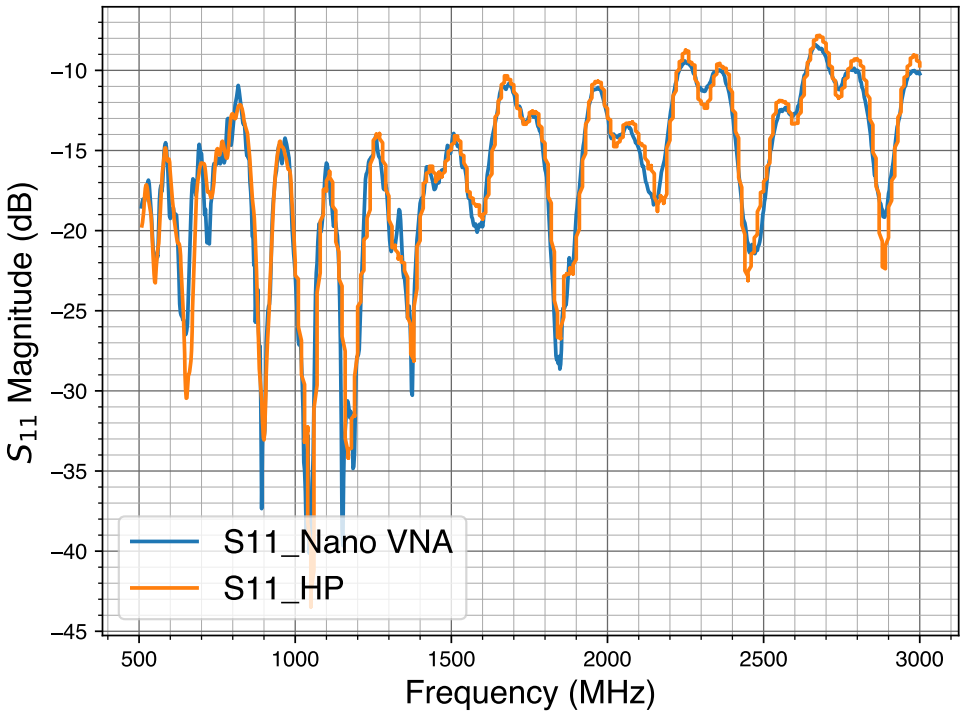

Figure 3.1: Reflection coefficient measurement of an antenna used to compare the NanoVNA and the HP 8720ET measurement similarities.

The S_{11}, or reflection coefficient, looks at the power reflected from the DUT, which, in the case above, was the LPDA antenna to be characterised. The measured response correlates well for both measurement devices.

3.2.1 Log-Periodic Dipole Array Antenna

Log periodic array antennas were first discussed in the 1950s by DuHamel and Isbell (1957) with Isbell (1960) exploring the use of dipoles in these arrays. Kibona (2013) describes this type of antenna as "a broadband, multi element, directional narrow-beam antenna that has impedance and radiation characteristics that are regularly repetitive as a logarithmic function of the excitation frequency". The specific antenna to be tested is A-INFO's DS-18300 LPDA characterised for a frequency range from 0.18-3.0 GHz. An image of the antenna, taken from the specification sheet A-INFO (2018), is shown in Figure 3.2.

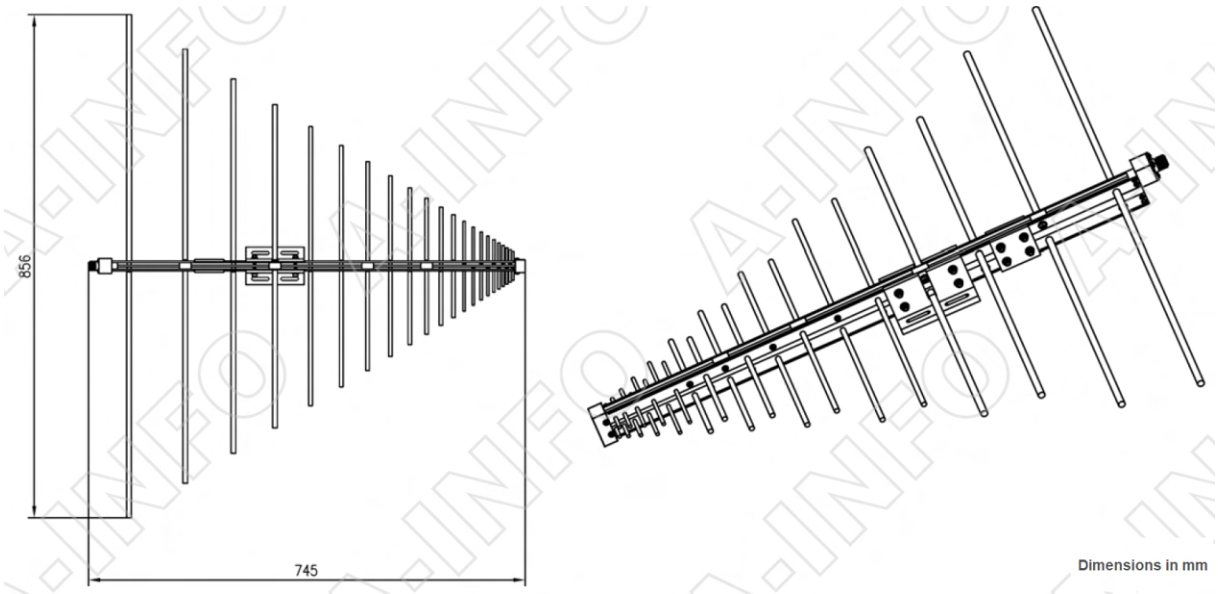

Figure 3.2: A-INFO's DS-18300 0.18 - 3.0 GHz log periodic antenna. Image taken from (A-INFO, 2018).

The electric field lines are always parallel to the radiating elements. When the antenna is mentioned as horizontal (H-Pol), this will be considered as the elements and E-field being parallel to the ground plane.

3.2.2 LPDA Phase Centre Considerations

The LPDA is split into three regions: the transmitting, active and non-active regions according to Balanis (2016). The active region, or phase centre, varies with respect to frequency. When considering the A-INFO LPDA (the antenna to be tested), the phase centre could shift by over 700 mm per antenna. This means that at the low frequencies, the separation distance R is roughly 1.4 m further apart than the high frequency point.

By running a simulation in Altair FEKO (2021) across the frequency range, with a request for currents, allowed a visual representation of this phase centre movement (Figure 3.3). The setup of the FEKO model is discussed in Section 3.6. Once three key areas and the respective frequency ranges had been determined, an *if* statement was incorporated into the Python code to use different separation distances, depending on the frequency, to calculate the gain.

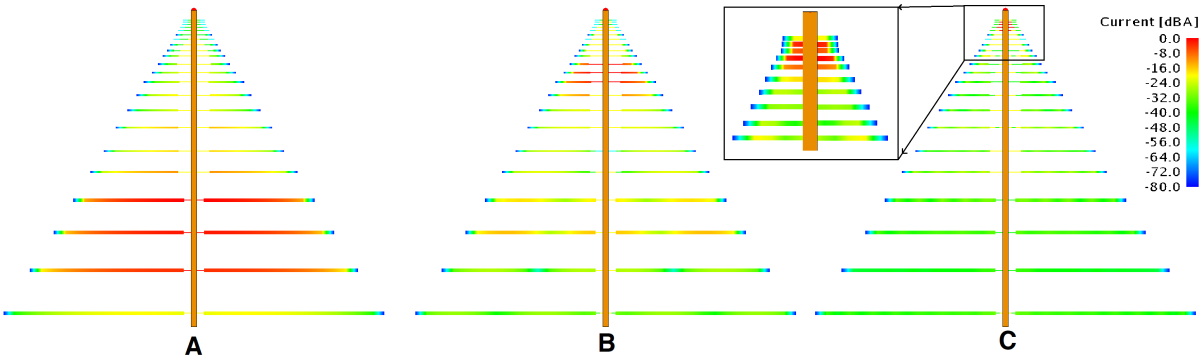

Figure 3.3: Normalized currents on the LPDA antenna as seen in FEKO at A = 231 MHz, B = 750 MHz, and C = 3 GHz. Red elements exhibit high collection of currents which show area (point) of propagation.

The separation distance was measured between the antenna mounts, therefore, for a separation distance of $R = X$ m, the lower frequencies (up to 231 MHz) radiating from the back elements used a separation distance of $R = X + 0.25$ m. Those radiating from the middle elements (231 - 750 MHz) used $R = X - 0.4$ m, and those radiating from the front elements (750 MHz - 3.3 GHz) used $R = X - 0.6$ m to account for the shifting of the phase centre.

3.2.3 Far Field Considerations

Due to the size and broad frequency range of this antenna, the required far field (FF) separation distance quickly increases with frequency. Using Equation 2.3 and the chosen antenna with a *D* of 0.856 m, Figure 3.4 was produced. This illustrates that to satisfy the FF equation will require a separation distance of 14.5 m at 3 GHz.

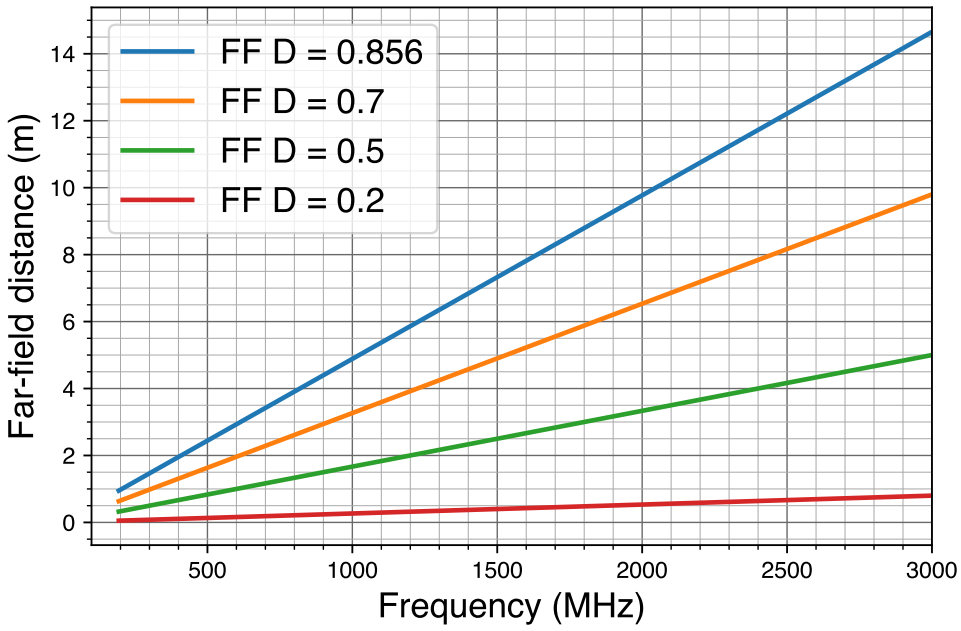

Figure 3.4: A-INFO's DS-18300 far-field distance with respect to frequency. DS-18300's *D* is 0.856, while D of 0.7, 0.5 and 0.2 are added for comparison.

The cables available for measurement are both 5 m long. Accounting for the change in height and sufficient distance for the measurement equipment, the maximum achievable separation distance with these cables is 8 m when boresighted. This equates to a FF frequency of 1.65 GHz when R = 8 m. The FF calculation, as discussed in Section 2.2.1 is not precise, but is rather an approximation. Part of this research will investigate the accuracy of the measurements when the antennas are closer than the far-field distance. An advantage of short cables and separation distances is that the measurement remains within the 60 dB of dynamic range achievable by the NanoVNA.

3.2.4 Non-Conducting Tripod Design

Parasitic coupling and detuning effects can occur when an antenna is operated near metallic objects. It is, therefore, good practice to ensure that there are no reflecting or conducting materials near the AUT. For this reason, a simple, rotatable, RF transparent tripod was designed to hold the antenna.

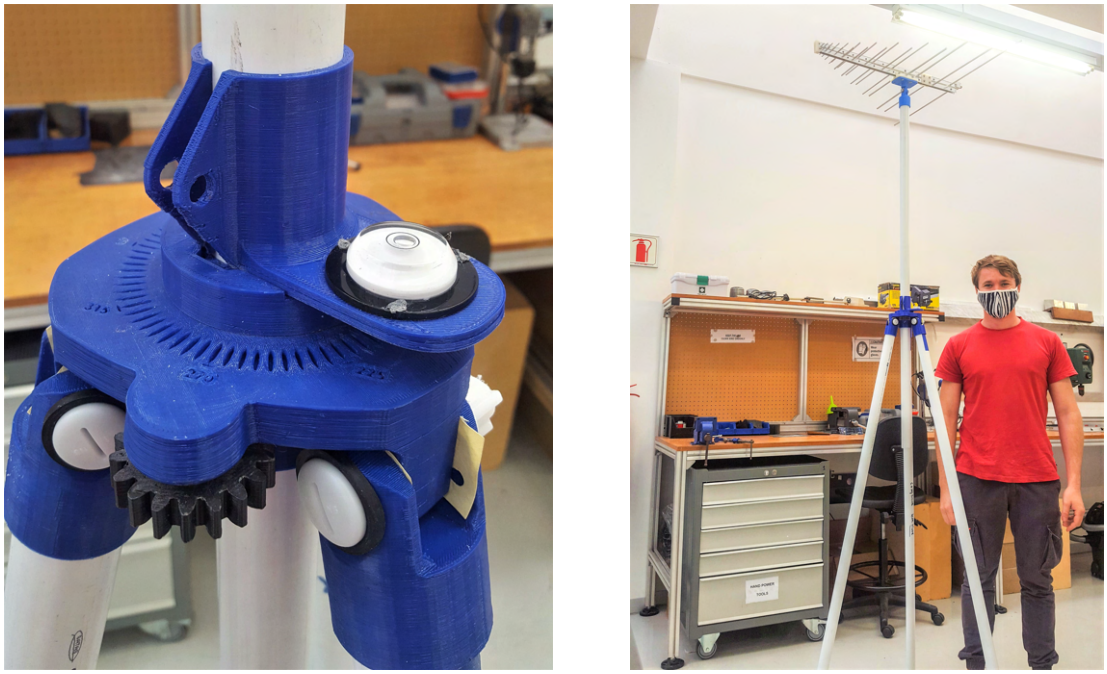

(a) **(b)**

Figure 3.5: (a) 3D printed tripod mechanism showing 5° increment marks. (b) One of the tripods and antenna in a CPUT lab.

It was designed to have intricate parts 3D printed and uprights cut from 50 mm PVC piping. The design was drawn up in Dassault Systèmes' SolidWorks, a computer-aided design (CAD) package. Figure 3.5 (a) shows the 3D printed mechanism for rotating the antenna with 5° increment marks. While (b) shows the tripod extended to a height of 2.9 meters with the antenna attached.

3.3 Analysis and Interpretation of Data

Many data files were created during the experiments and simulations. To distinguish between data files, a naming convention was predefined as follows: *2mt_2mr_h_3m.s2p*. The *2mt* is for the transmit antenna height, while the *2mr* is for the receive antenna height: both being 2 meters high in this case. The *h* is to inform that the antenna elements were horizontally polarized (v if they were vertical) and the final *3m* is for the separation distance of 3 meters. Each individual VNA's measurements were saved into a separate folder. Gain pattern measurements were saved into individual folders named to the convention as discussed above, with each file labelled by its angle (e.g., *0deg.s2p, 5deg.s2p, 180deg.s2p*).

3.4 Gain Calculation

Using the Python code shown in Appendix D.1 the *.s2p* files consisting of the measurements at angle 0°, 5°, 10° etc. were written to one .xlsx file with each angle on its own sheet. The code below (see Appendix D.2 for full code) then used a *for loop* to convert all the different transmission parameters (S_{21}) into the respective gains using Equation 2.9.

```
for ws in wb.worksheets:
    sheet = -1 # set sheet number start
    sheet = sheet + 1 #Increment sheet number
  if sheet >= 25: #if sheet is bigger than 25 (120 degree)
      sd3 = 3       #Standard distance
      df3 = sd3 - 0.14   #Distance far
      dm3 = sd3 + 0.2  #Distance middle
      dn3 = sd3 + 0.35   #Distance near
  elif 10 <= s < 25: #if sheet is between 10 (45 degree) and 25
      sd3 = 3
      df3 = sd3
      dm3 = sd3
      dn3 = sd3
  else: # if sheet is less than 10 (45 degree)
      sd3 = 3
      df3 = sd3 + 0.14
      dm3 = sd3 - 0.2
      dn3 = sd3 - 0.35

  for i in range(rowS, rowF): #Sheet start row and final row for operations
      LMag = ws.cell(row=i, column=2).value
      Wl = ws.cell(row=i, column=5).value
         if Wl >= 1.3: #Using wavelength w.r.t propagation point
         R = df3
         elif 0.4 <= Wl < 1.3:
```

```
            R = dm3
            else:
            R = dn3

        GL = ((LMag*4*np.pi*R)/Wl)  #linear gain calculation
        G = 10*(m.log10(GL)) #Liner to dB gain calc
        ws.cell(row=i, column=6).value = GL #Storing linear gain values
        ws.cell(row=i, column=7).value = G  #Storing dB gain values
```

This code loops through the sheets in the workbook and applies the calculations. It accommodates the change in R as the separation distance changes with rotation angle. For example, at 90° all radiating elements are orthogonal to the other antenna and hence at the same distance. The point of propagation with respect to frequency was also accounted for.

3.5 Houwteq OATS Measurements

The Houwteq OATS is based 70 km from CPUT's Bellville campus. As this facility is not owned by CPUT, permission to use the facility was requested in advance. CPUT's HP 8720ET VNA is not user-friendly off-site as it does not have a carry case and requires a specific desktop to save measurement data. Instead, the South African Radio Astronomy Observatory's (SARAO) Rohde & Schwarz (R&S) ZVB8 was used. It has a safe carry case and allows data to be saved to a memory stick via USB. The consistent response from the OATS allowed comparisons of the different VNAs tested. This acted as a baseline for the sports field measurement comparisons.

(a)

(b)

Figure 3.6: (a) A-INFO LPDA and tripods as seen at Houwteq's OATS. This site with its flat metallic surface acts as a reflection range. The building seen here is made of RF transparent material. (b) Attending to connectors while warming up the R&S ZVB8.

3.5.1 OATS Measurement Setup

The building on the OATS allowed for a sheltered place to setup the equipment. Being made from fibreglass and plastic it is RF transparent, and therefore, will not affect the measurements. The transmit and receive antennas were setup outside of the building with the VNAs inside as shown in Figure 3.6. The layout, depicted in Figure 3.7, ensured the least possible multipath reflections by pointing the transmit antenna (Antenna 1) away from any possible reflection planes, boresighted at the receive antenna.

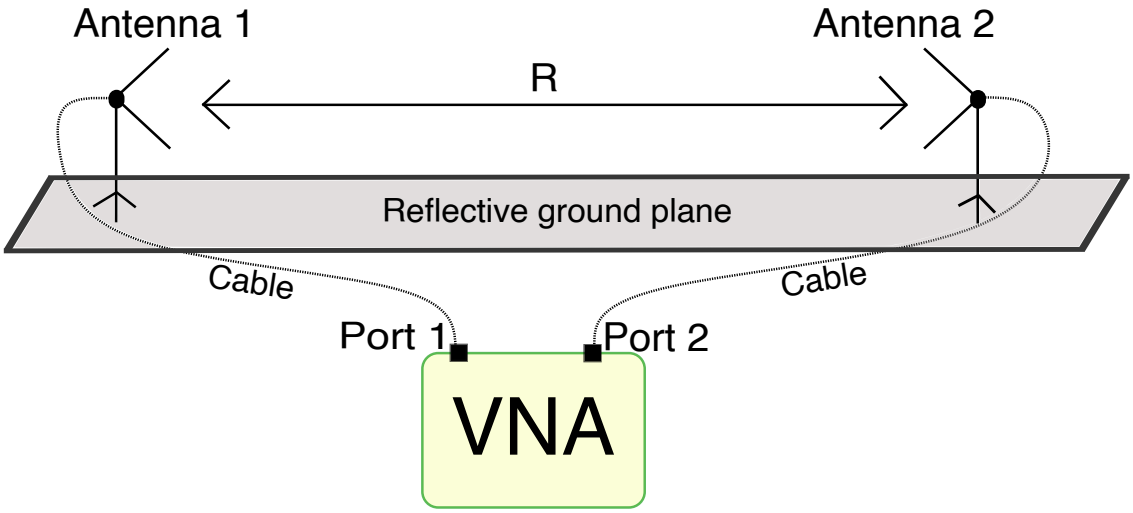

Figure 3.7: Layout of antennas and VNA at Houwteq test site. Showing the VNA with respect to transmit and receive antennas in addition to the cable.

3.5.2 Measurements

Care was taken with all measurements to ensure that all connectors were clean and properly torqued. The VNA was always sufficiently warmed up and routinely re-calibrated to prevent drift errors. Calibration was done over a frequency range of 150 MHz - 3.1 GHz with 601 measurement points. This calibration allowed the VNA to mathematically remove the response of the cables and connectors up to the point where the antenna would be connected, known as the reference plane.

The Rohde & Schwarz ZVB8 took an average of 40 seconds from the start of scanning to saving a measurement file. This was repeated for several combination of Tx and Rx antenna heights before taking the gain pattern measurements. These measurements were done in horizontal polarization by turning the Rx antenna through 5 degrees (as marked on the tripod, Figure 3.5 (a)) up until 180 degrees, giving 37 measurements for one gain pattern. The measurement sequence was repeated for vertical polarization. Once all the measurements for R = 3 m were complete, the separation distance was changed to 5 m and the process repeated.

After completing measurements with the ZVB8, CPUT's NanoVNA V2 was used to take measurements. This VNA was the slowest of the three taking on average 2.25 minutes from beginning scanning to saving a measurement file. Control of the NanoVNAs is possible via a laptop program, which communicates over USB. There are several open source applications available for controlling the device, however, the manufacturer-recommended *vna_qt.exe* software was used.

MESA Solutions' NanoVNA V2 Plus4 was experienced as the fastest device, completing the process of scanning and saving a file within 25 seconds. Only faster than the ZVB8 due to the ease of saving in the *vna_qt.exe* software.

The photographs in the figures below show a comparison between the VNAs: CPUT's being the smallest NanoVNA seen in Figure 3.8 (a), a phenomenal difference when compared to the ZVB8 in (b). The NanoVNAs weigh less than 350 grams while the ZVB8 weighs 18 Kgs. The low weight and small size of the NanoVNA gives a large portability advantage over commercial VNAs, allowing for easier in-field testing.

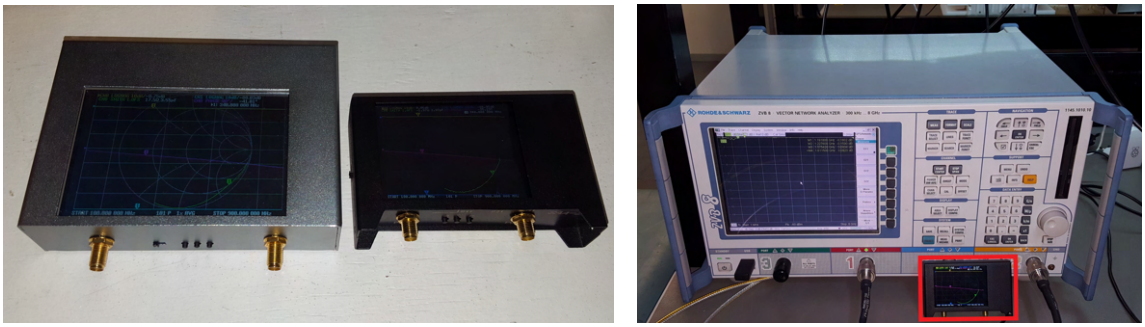

(a) **(b)**

Figure 3.8: (a) NanoVNA V2 Plus4 (Grey) next to the NanoVNA V2 (Black). (b) Rohde & Schwarz ZVB8 behind the NanoVNA V2 (lower right box in red).

3.5.3 Results and Discussion

The reflection coefficient of an antenna is the least easily influenced parameter, making it easily repeatable. This makes it ideal for comparing the different VNAs as the antenna response is unlikely to change for the same setup. Figure 3.9 shows the reflection coefficient of the same antenna 2 m above the OATS metal ground plane. The plot shows that the different VNAs track within 1 dB of each other for the majority of the measurement with the most significant difference (12 dB) being at 1000 MHz. At this frequency, the ZVB8 shows the least antenna reflection, most likely due to the high-quality calibration kit and better dynamic range capabilities of the ZVB8. The NanoVNAs give very similar results across the band, with a 5 dB difference at 1350 MHz where the NanoVNA V2 shows less reflection.

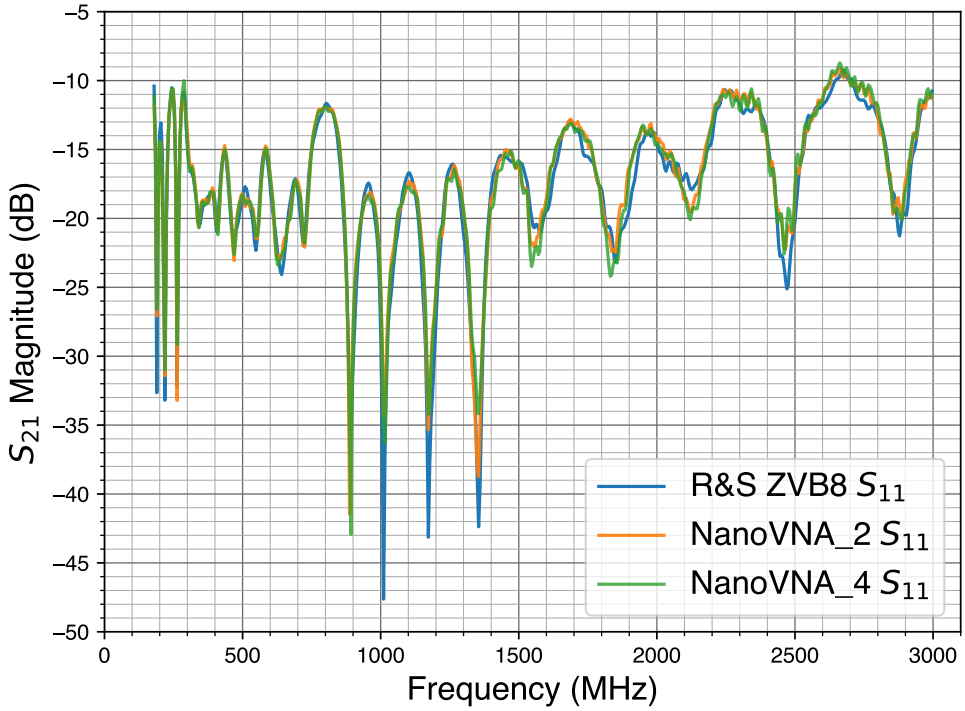

Figure 3.9: A-INFO LPDA's S_{11} as measured by the ZVB8, NanoVNA V2 (NanoVNA_2) and NanoVNA V2 Plus4 (NanoVNA_4) at the OATS.

This S_{11} response is typical of an LPDA, with the dips representing element length resonance.

Reflection and Transmission Plots

The following figures show the VNA data captured for the transmission coefficient (S_{21}). This is different to the reflection coefficient as the one antenna transmits while the other receives. This means that the distance between the antennas should be as similar as possible when changing VNAs. Figure 3.10 (a) and (b) shows the S_{21} response when separation distance (R) = 3 and 5 m respectively.

Much like the S_{11}, the devices achieve similar results across the band, with the ZVB8 achieving slightly deeper troughs due to its improved dynamic range and high-quality calibration kit. The NanoVNA V2 achieved slightly higher peaks due to shorter separation distance. This difference is also apparent due to the rightward trend shift seen in the response for the ZVB8 above 2000 MHZ in Figure 3.10 (a).

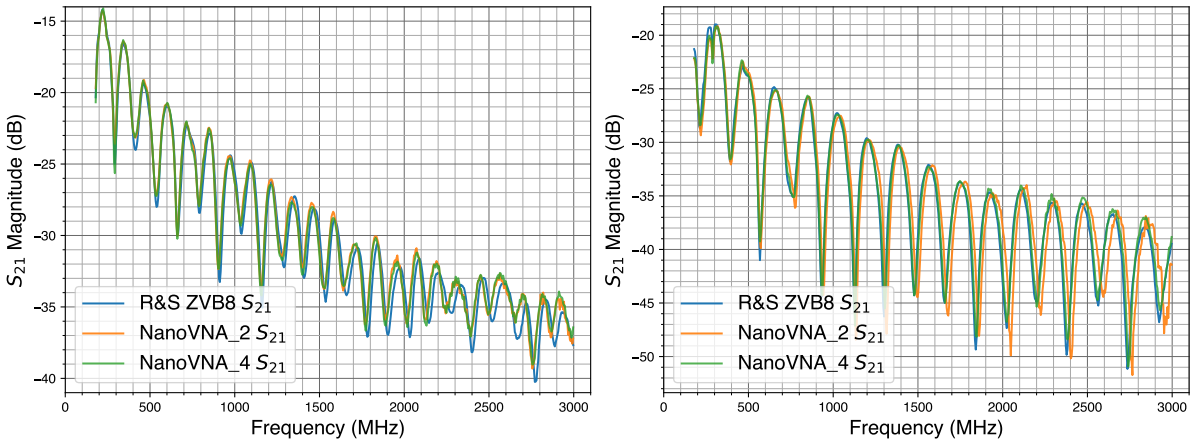

Figure 3.10: A-INFO LPDA's S_{21} as measured by the ZVB8, NanoVNA V2 and NanoVNA V2 Plus4 (NanoVNA_4) with a (a) 3 m and (b) 5 m separation distance.

A change in R will alter the point of reflection. This in turn changes the arrival phase difference of the direct and ground reflected waves. This is more prominent in the higher frequencies due to the shorter wavelengths. The results in Figure 3.10 (b) agree with this statement as the shift is seen for the NanoVNA V2 and not the ZVB8.

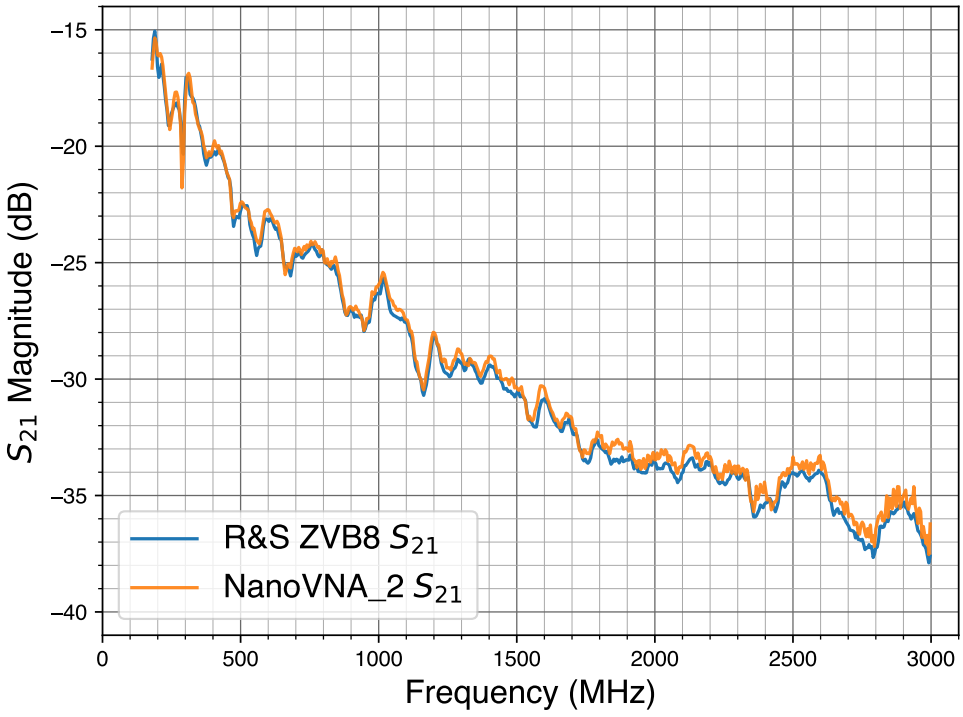

Figure 3.11: A-INFO LPDA S_{21} measured in V-Pol by the ZVB8 and NanoVNA V2 at the OATS.

The vertical polarized (V-Pol) measurement results (Figure 3.11) do not produce the same oscillating effect as seen in the horizontal polarization. This is due to the E-field variation direction with respect to the ground plane. For horizontal polarization the reflected varying E-fields can add exactly in- and out-of-phase, as is shown by the results. In vertical polarization

the phase is scattered more and does not show this same trend. Boresight measurements highlight many factors of antennas in one measurement, the polar pattern, however, is achieved by stitching many subsequent measurements together to form one plot.

Polar Plots

The polar plots were accomplished by incrementally changing the angle of the receive antenna by 5°. These 5° increments were repeated up to 180°. A clockwise direction was selected as it turns the receive antenna away from the measurement equipment which could affect the results. Measurements up to only 180° were done to half the required measurement time. This will not affect the polar plots significantly as the AUT is near symmetrical across the feed line. Therefore, although the polar plots are shown as 360° the half pattern is merely mirrored.

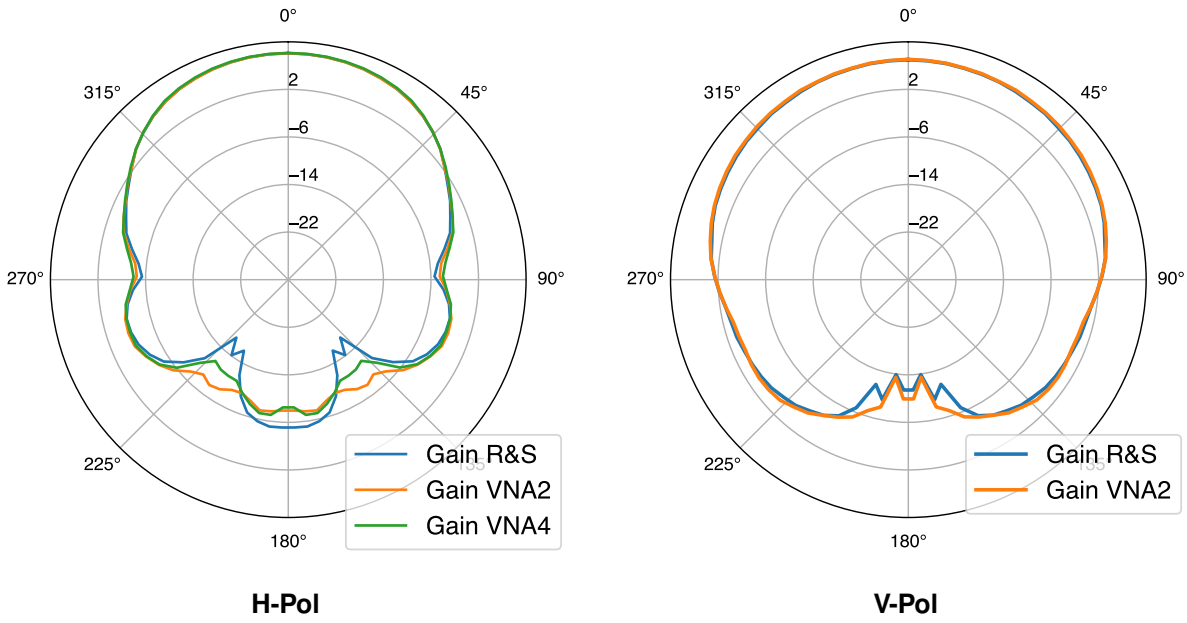

H-Pol **V-Pol**

Figure 3.12: A-INFO 600 MHz gain pattern measurement comparison for NanoVNAs and ZVB8 on the OATS with a separation distance of 3 m.

The H-Pol patterns illustrated in Figures 3.13 and 3.12 show good pattern correlation, however, the R&S measures more gain in the main lobe (315° - 45°) at 1.5 GHz. This increase in gain is attributed to the slight difference in separation distance causing the RF waves to add more in-phase at 1500 MHz. This is not seen on the 600 MHz trace as the longer wavelength is not as affected by small differences in R. The NanoVNAs respond within 0.5 dB of each other for the majority of the measurement.

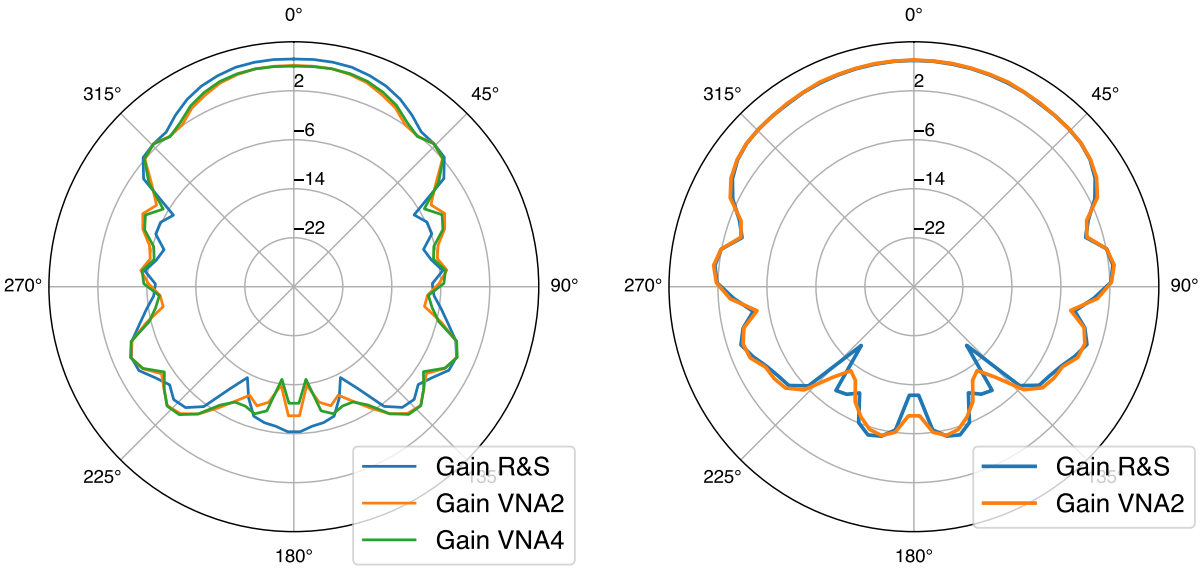

Figure 3.13: A-INFO 1.5 GHz gain pattern measurement comparison for the NanoVNAs and ZVB8 on the OATS with a separation distance of 3 m.

The V-Pol patterns shown complement previous findings with the results showing close correlation between the VNA V2 (VNA2) and the R&S, with the only visible difference seen in the back lobe. The back lobe differences are attributed to the lower dynamic range achievable with the R&S and possible differences in the cable layout as it leaves the antenna. The V-Pol shows only the R&S ZVB8 and NanoVNA V2 as there was insufficient time to make the required pattern measurement with the NanoVNA V2 Plus4 (VNA4).

3.5.4 OATS Conclusion

The measurements taken at the Houwteq OATS resulted in three main findings;

- Firstly, they allowed the individual VNAs to be compared across multiple measurements, showing that the NanoVNAs can be used successfully in the place of commercial equipment for these type of measurements without compromising accuracy.
- Secondly, they acted as a baseline for a commercial OATS response which will later be compared to the sports field's response.
- Thirdly, they allow for a PEC ground plane to be used when comparing to FEKO simulations to ensure simulation accuracy to real world results.

These results answer part of the first Research Objective (1) in that NanoVNAs can be used to cost-effectively characterise UHF antennas.

3.6 FEKO Modelling and Simulation

3.6.1 Introduction

With the capability of available computational electromagnetics (CEM) modelling software, various use cases for an antenna can be tested in a simulated environment. Having this ability allows an extra level to be added to the testing methods being discussed here. Once actual measurements had been taken of the antenna, the simulation software by Altair FEKO (2021) was used for modelling. In this section the modelling, simulation and extra testing of the A-INFO antenna's results are discussed.

3.6.2 CAD Considerations and Setup

CAD FEKO was used to model the antenna. As there were no detailed dimensions available for the A-INFO LPDA, all 22 of the elements lengths and spacing were measured and modelled as accurately as possible. Due to the mirrored and flipped design of the LPDA, focus was given to drawing one half. The remaining half was produced by a mirror and flipped duplicate transform function. The LPDA model with wire elements prior to meshing can be seen in Figure 3.14.

Wire elements were used instead of cylinders due to lower computational effort required to complete a simulation. Wire element simulations completed in a fourth of the time required for cylinders without a significant change in the reflection coefficient. When drawing, each wire was given a radius to apply during meshing. As this was drawn from a real world model, matching the simulated results to the real world measurement was required, therefore, a faster simulation time to test, compare and change was advantageous.

The machine available for running simulations consisted of two Intel(R) Xeon(R) CPU E5-2630 v4 at 2.2GHz. This gives a combined value of 20 cores and 20 logical processors. It also boasted 64 GB of available random-access memory.

Meshing

Techniques such as the MoM solver in FEKO use meshing to discretise the currents throughout the model. Essentially breaking them down into smaller, computable sections. As the sections get smaller, accuracy increases along with the required computational resources and simulation time. The default mesh sizing consisted of *"segment radius to length is too large"* error which referred to the length of the wires compared to the given thickness applied to the dipole elements.

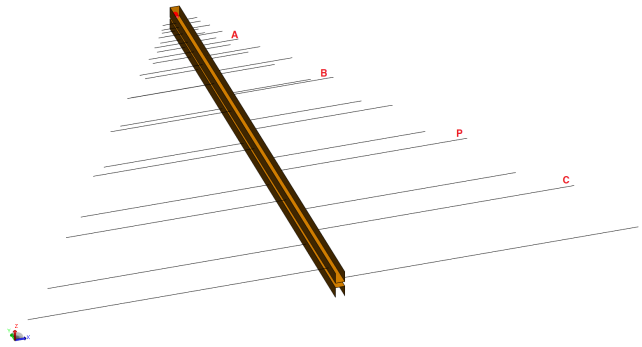

Figure 3.14: CAD FEKO model used for simulations. Elements displayed as wires with phase-centres marked A - C. P is the fixture point where separation distance (R) was measured from.

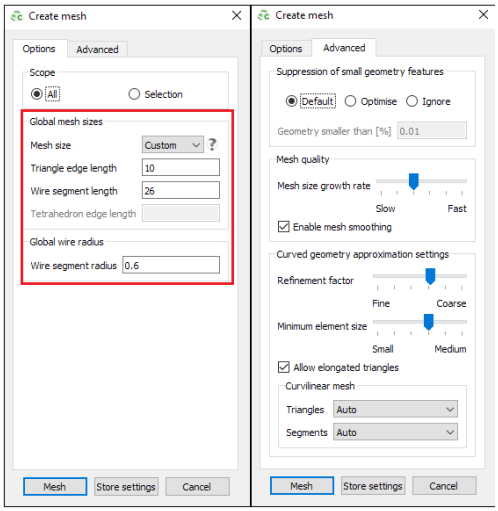

Figure 3.15: CAD FEKO model mesh settings. Showing global mesh sizes (red box) and advanced settings. This allowed the long wire elements to be simulated without an error.

Due to the error, mesh settings shown in Figure 3.15 were applied. This consisted of a global mesh size with triangular edge length of 10 mm and a wire segment length of 26 mm, which allowed successful validation of the mesh.

Ground Plane

FEKO allows for an infinite ground plane to be added at $Z = 0$. This was done initially as a perfect electric conducting (PEC) ground plane to allow comparison to the OATS results. The S_{21} response (used to calculate gain) was achieved by adapting the CAD design to have two identical antennas bore-sighted as seen in Figure 3.16. A request for *Multiport S-Parameter* was then added to the model, allowing the simulation of the antennas in the same fashion as the OATS. The soil characteristics were added by means of reflection coefficient approximation (RCA).

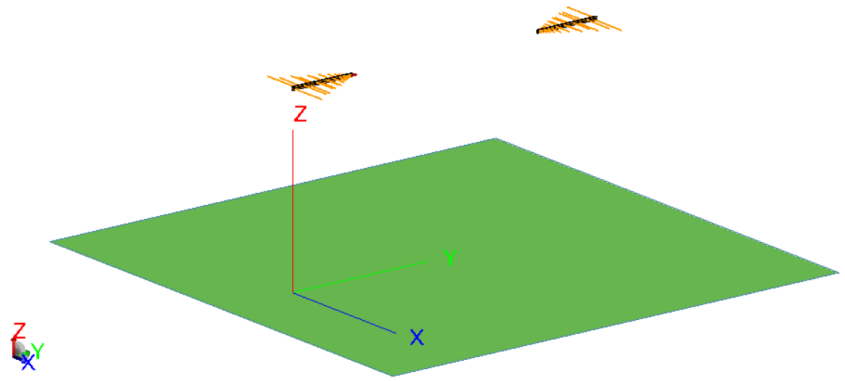

Figure 3.16: Two modelled antennas above an infinite ground plane as seen in Altair FEKO (2021).

The model seen in Figure 3.16 shows two antennas above an infinite RCA ground plane.

The RCA adds a reflected component to the simulated fields, improving similarity to real world results. The soil characteristics discussed in Section 2.7.1 were applied to the model. This gave a different response to the PEC ground plane as shown in Figure 3.17 below. The different S_{21} achieved when simulating with PEC; soil under exact Sommerfeld integrals (SFI); and RCA methods are also shown.

Optimisation is a key factor for these simulations. The difference between the SFI and RCA solution is indistinguishable in Figure 3.17, however, simulating the 601 points took over 25 hours for the Sommerfeld integrals while the RCA result took only 10 hours.

3.6.3 Simulation

Element length and spacing accuracy was crucial to match the model to the measured results for this complex antenna. The results can be seen in Figure 3.18, which also shows the similarity in the trend of the simulated PEC ground to the two antennas tested at the OATS. The orange and green traces are the two A-INFO LPDA antennas. Although they were manufactured together, the response is not perfectly identical. The traces correspond well throughout the frequency range with an exception at 1500 MHz where the actual measurements show a more resonant feature that does not occur in the simulation.

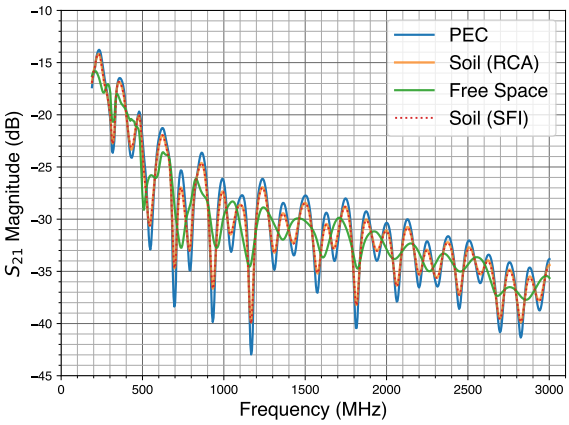

Figure 3.17: FEKO S_{21} H-Pol response when comparing three different ground planes and RCA compared to SFI.

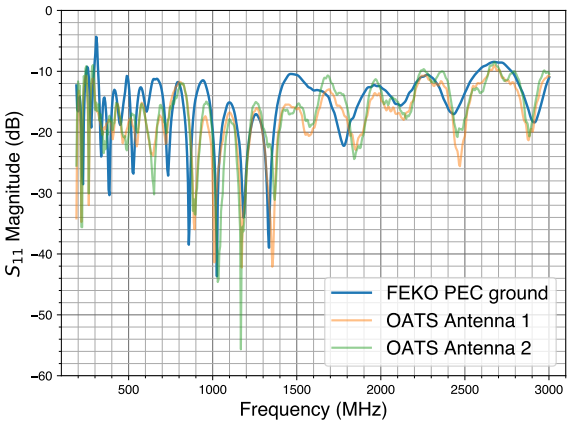

Figure 3.18: FEKO simulated S_{11} at h = 2 m, compared with the two identical antennas measured S_{11} at the OATS.

Displayed in Figure 3.17 are the different horizontal polarization transmission responses for different ground planes. The PEC ground plane (blue) shows higher peaks and deeper troughs due to the increased signal reflections. The reflected waves add in and out of phase with the direct wave at the receive antenna, causing the oscillating pattern. Due to the absorbent properties of the soil, the phase addition was not as extreme as the PEC, and therefore, the

peaks and troughs are less prominent. The response of the soil was identical for both SFI and RCA.

The free space response (green) shows the response of the antenna with no ground plane. The peaks and troughs for this transmission are due to the design parameters of the LPDA, mainly, the impedance characteristics. Balanis (2016:607) discusses that as the element spacing decreases at the higher frequencies, the variation in impedance and other characteristics decreases due to the smoother transmission of the active region (where elements $\approx \lambda/2$) between the closer elements. This is visible with the increase in frequency whereby the trace stabilised more. For instance, at 500 MHz there is an 8 dB variation while at 2000 MHz the variation is roughly 3 dB (see Figure 3.17).

3.6.4 Simulation Polar pattern

OPTFEKO is used to optimize simulation parameters, it can also be used to run a function on a model. This was used to turn one of the simulated antennas through 180° in 5° increments. Performing a similar test to the OATS polar pattern measurements made in Section 3.5.3. The results can be seen in Figures 3.19 and 3.20. FEKO has a 3D polar pattern request which was used to show the simulated patterns in Section 4.5 and to create the 3D far-field pattern illustrated in Appendix B.

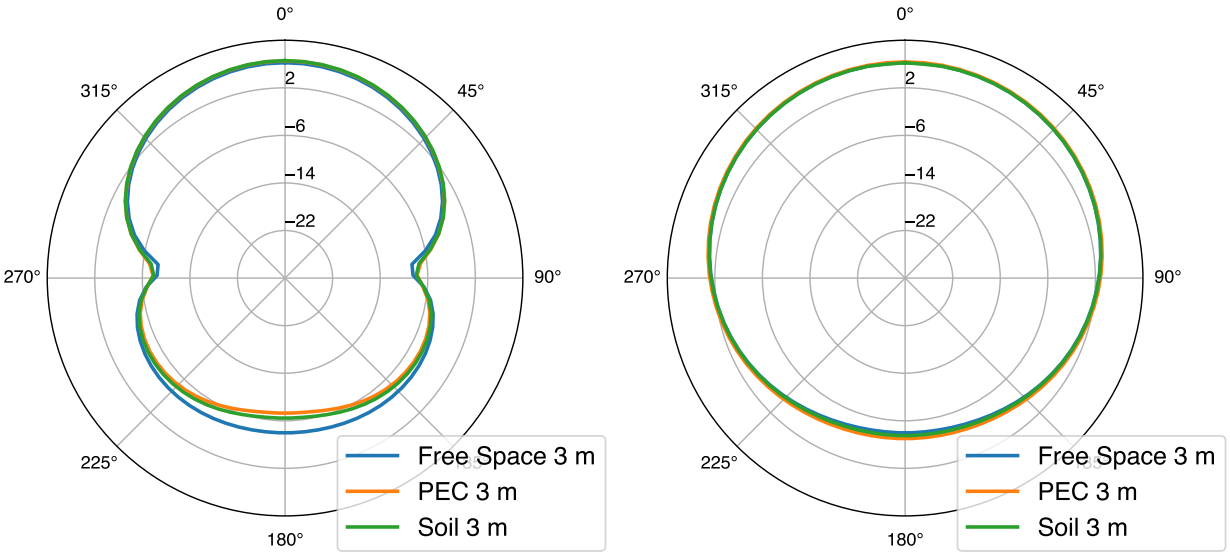

Figure 3.19: Simulated gain pattern using OPTFEKO with a separation distance of 3 m at 200 MHz for H- and V-Pol.

Figure 3.19 shows that at lower frequencies, the difference in the RCA ground plane response is less distinguishable for the majority of the plot.

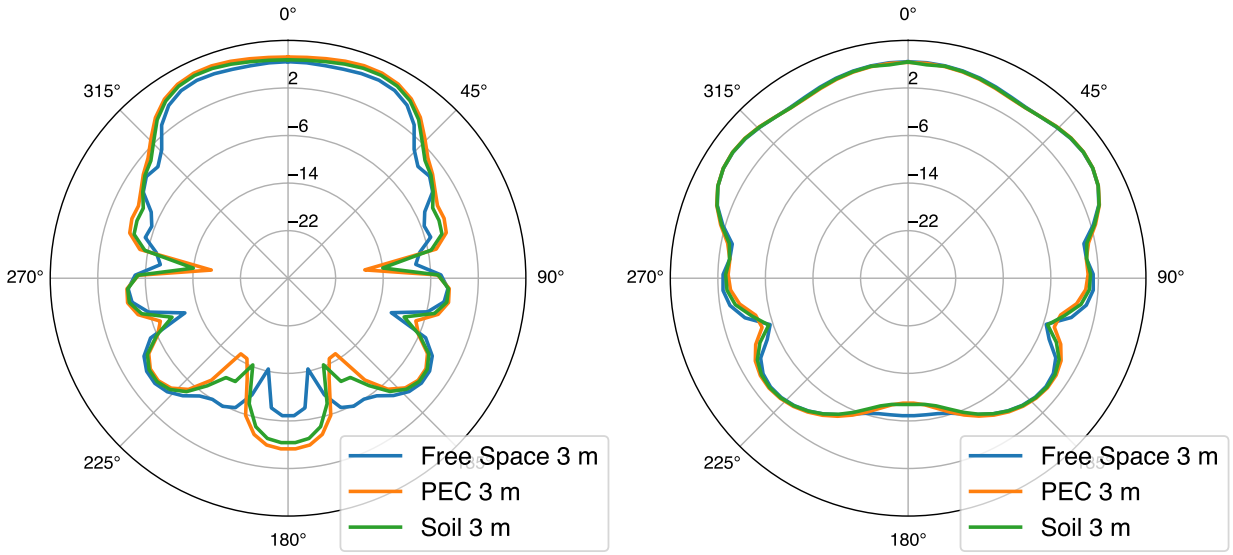

Figure 3.20: Simulated gain pattern using OPTFEKO with a separation distance of 3 m at 1.5 GHz.

Figure 3.20 shows that for the H-Pol, a slight decrease in gain could be expected above a soil ground plane compared to the PEC ground plane. The pattern, however, is not adversely affected by the presence of a different ground plane. The V-Pol, which is not as affected by the ground reflected wave, shows strong correlation for all three measurements at both 1.5 GHz and 200 MHz.

3.6.5 Conclusion

Being able to simulate the response of different ground planes showed that, in the presence of a soil ground plane, more of the incident radiation was absorbed. This is seen best with the S_{21} trace shown in Figure 3.17. The polar patterns confirm that the absorption from the ground plane does not adversely affect the shape of the polar pattern for both the H-Pol and V-Pol. It does, however, decrease the measured gain experienced with the soil ground plane due to partial absorption of the reflected wave. The V-Pol simulations show that due to the minimal effect of the ground plane in this orientation, the patterns are similar to the free-space simulations. These findings support the hypothesis that a sports field could be used as a reflection range, showing that the difference between the PEC and soil response could be expected to be less than 1 dB on average.

3.7 Sports Field Measurements

Sports fields allow easy access to large open areas consisting of a flat ground plane. These are in theory not ideal antenna test ranges due to the likely reflections from nearby structures such as podiums and signage. Possible background interference can also play a negative role in the measurement results as the background environment is likely RF noisy. In this section, an investigation into antenna measurements on a sports field using equipment proven at the OATS to be accurate, will be conducted. This will take into account possible multipath reflections and measurements of background noise that could negatively affect the results.

3.7.1 Measurement setup

Similar setup considerations as with the OATS were taken for the sports field. Pointing the transmit antenna away from any metallic surfaces, with the receive antenna rotating in the direction of least possible reflections. The setup can be seen in Figure 3.21, using the middle of the field to ensure all large reflection planes (except the ground plane) was over 45 m away. As a wave would need to travel to the reflection point and back, this distance is doubled to 90 m, far more than the 3 to 8 m separation distance tested.

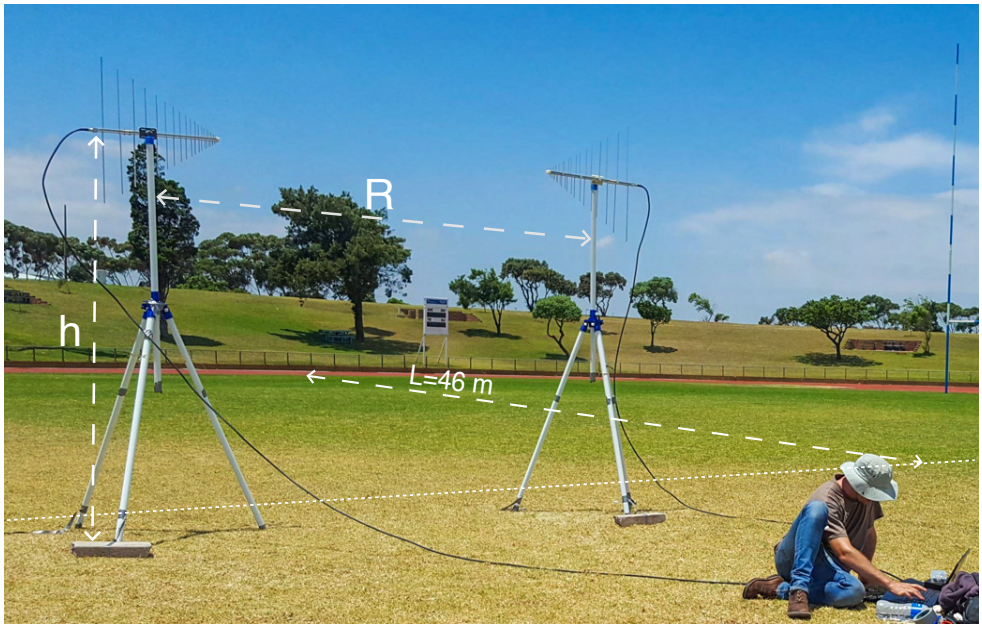

Figure 3.21: Sports field testing with antennas in vertical polarization, h = 2 m, R = 3 m. The setup was in the middle of the sports field with the distance to barrier (L) being 46 m.

A Tektronix RSA306B USB real time RF spectrum analyser was used to scan the RF background spectrum. There was significant noise in certain bands, however, the 1000-1700 MHz was quiet as seen in Figure 3.22. The signal at 950 MHz is due to a nearby cellphone tower.

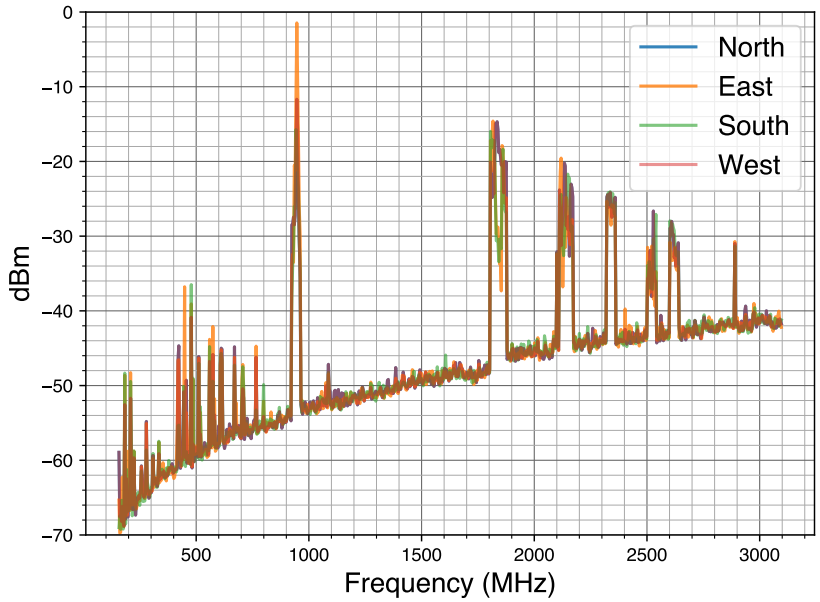

Figure 3.22: Sports field background noise power measurement results, accounting for antenna factor and cable losses.

Knowing the background spectrum ensures that any unexpected spikes on the measurement results can be correlated to the environment if required. Knowing the quiet region of the spectrum will ensure that the results from that section are untainted, and therefore, preference will be given to the 1 GHz, 1.5 GHz and 2 GHz measurement responses.

3.7.2 Results

Having proved with the OATS measurements that the NanoVNA gives corresponding results to a commercial VNA, the NanoVNA V2 was used for all sport field measurements.

Boresight Response

The transmission results for H-Pol and V-Pol are shown in Figure 3.23. The *2.5mt2.5mr_2m* trace in H-Pol shows the least fluctuation due to the closeness and height of this setup. The reflection path is nearly twice the length of the direct path. This theoretically causes a free-space transmission, which is ideal for the testing, but does not meet the far-field criterion for frequencies above 400 MHz. As the antenna separation increases the reflected wave becomes more apparent. The moisture of the soil was more in *2mt2mr_2_3m* than in *2mt2mr_1_3m*. Due to the higher soil moisture content, the permittivity was increased, which in-turn decreased the amount of reflection. This can be seen by the more exaggerated peaks and troughs of *2mt2mr_1_3m*. The *2mt2mr_8m* shows the increased role of the reflected wave as the separation distance increases.

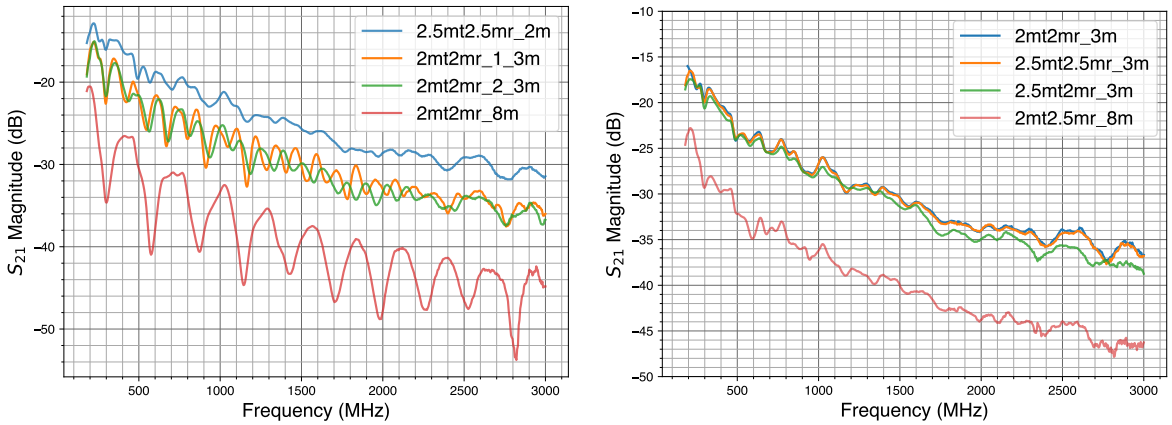

H-Pol **V-Pol**

Figure 3.23: Transmission response over an array of different antenna separation distances and heights on the sports field in both H- and V-Pol.

The V-Pol results do not interact with the ground plane as in the H-Pol, and therefore the response is more flat. The features, such as the drop at 500 MHz and the rise at 1050 MHz translates across the V-Pol traces and is also visible on the *2.5mt2.5mr_2m* H-Pol trace.

Polar Pattern

Using the NanoVNA V2 to make measurements, the patterns shown below for R = 3 m and 8 m were made. The H-Pol results seen in Figure 3.24 shows the largest gain difference between the 3 m and 8 m separation distances. The reason for this large change can be seen by looking at Figure 3.23 H-Pol. The 600 MHz frequency point shows a peak transmission for 3 m separation distance (orange trace) as the direct and reflected wave add constructively.

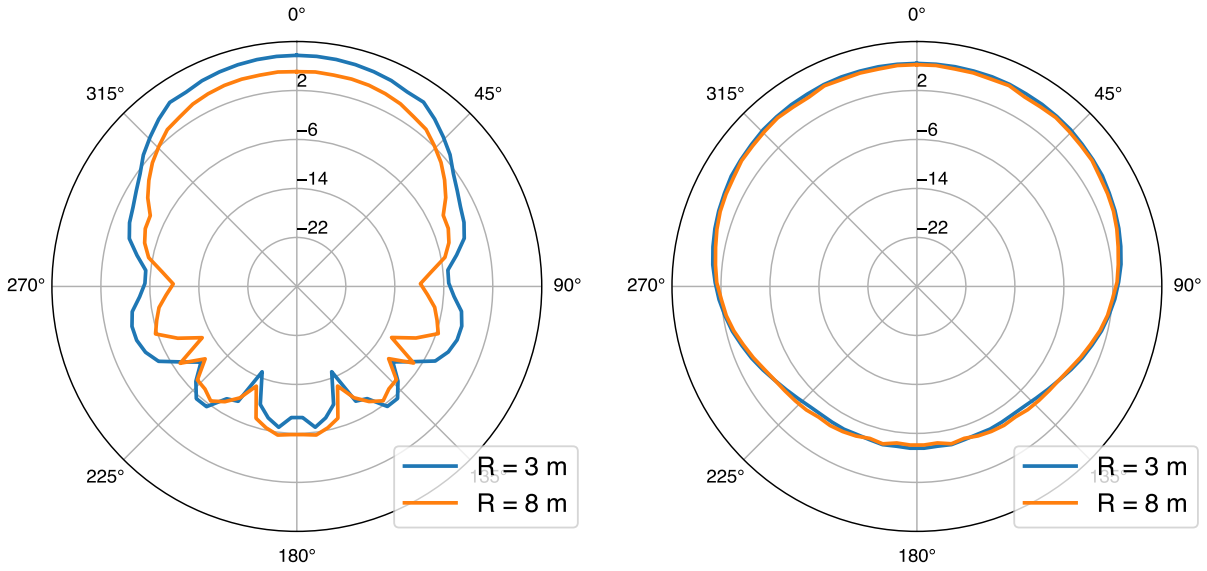

H-Pol **V-Pol**

Figure 3.24: Sports field H-Pol and V-Pol polar pattern of the A-INFO LPDA at 600 MHz for R = 3 m and R = 8 m.

For the R = 8 m trace, however, the received wave is in a trough due to the destructive adding of the multi path signal causing less gain for the majority of the measurement. As discussed earlier, due to the orientation of the E-field the V-Pol is not significantly influenced by the reflections. This is evident in both V-Pol plots seen in Figures 3.24 and 3.25 where the patterns are similar throughout the plot.

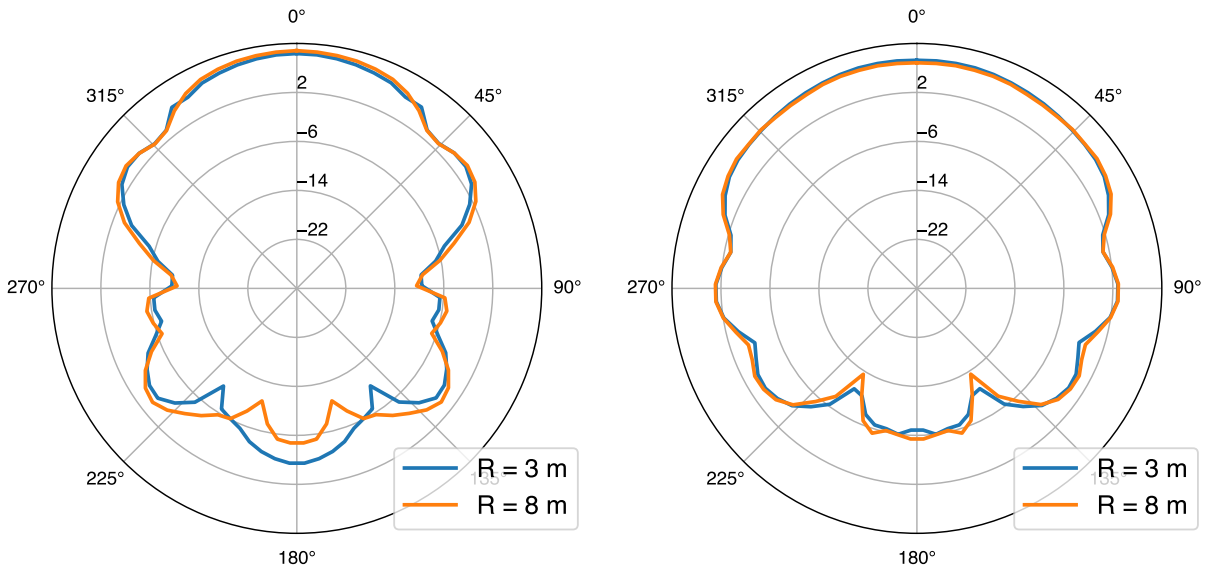

Figure 3.25: Sports field (a) H-Pol (b) V-Pol polar pattern of the A-INFO LPDA at 1 GHz for R = 3 m and R = 8 m.

The transmission response for 3 m and 8 m are both at peaks for 1 GHz. This results in a more correlated response for the horizontal polarization at 1 GHz (Figure 3.25) than at 600 MHz. The back lobe is likely affected by the cable protruding out the back of the antenna for this plot.

3.8 Conclusion

In this chapter, the transmission coefficient and polar patterns taken at two different antenna ranges and simulated have been presented and discussed. The results show that, using a NanoVNA, measurements can be made on the sports field. Changing the separation distance does, however, present discrepancies due to the summing of multi-path reflections as seen in Figure 3.24. In Chapter 4, the measurements between the OATS, simulation, anechoic chamber and sports field will be compared and discussed to quantify the level of accuracy realizable on the sports field.

Chapter 4

Result Comparison and Discussion

In this section, the results from the different measurement locations and simulations will be analysed and compared. Techniques to smooth the phase variance seen in the H-Pol will also be discussed and implemented using a Savitzky-Golay filter. Gain calculations will be made to show the gain results from the different measurements.

A special opportunity was granted late in the research to make use of the Houwteq anechoic chamber (see Figure 2.9). This range is cladded with radar absorbing material and is used to do standardized testing. The tests done at the anechoic chamber are considered the most accurate representation of the antennas response, however, the data sheet gain is also used as a comparative metric.

4.1 Assumptions and Limitations

The available cables did not meet the required separation distance to satisfy the far-field criterion as calculated in Section 3.2.3. Tests were conducted for different separation distances in FEKO, with similar gain responses between 15 m and 3 m (see Appendix C). Therefore, it was assumed that the results with R = 3 m were sufficient for these comparison tests.

The direct- and ground-reflected waves sum in horizontal polarization to give an oscillated response which could be de-embedded to diminish the response of the reflected wave. Using the V-Pol significantly decreases the role of the reflected wave, and therefore only the V-Pol values were used for calculated comparisons such as Table 4.1, 4.2 and 4.3.

The measurements used in this research were taken in summer. As the field is actively watered the soil conditions likely changed between measurement days as discussed in Section 2.7.1.

The Nano VNA V2 scan time is rather slow, therefore, only 601 points were selected across the frequency range.

As this research was conducted during the COVID-19 pandemic, the campus and sports field was not as active as usual. Therefore, access to the sports field was easier to attain and the level of RF background noise likely reduced.

4.2 Transmission Response

The transmission response for different antenna ranges and simulations are seen in Figure 4.1. The H-Pol and V-Pol correlate strongly for the sports field, OATS and anechoic chamber measurements, proving that the boresight measurements can be replicated with high precision at different ranges. The increased reflection off the OATS causes the in and out-of-phase summing to produce larger variations throughout the frequency range. This is easily visualized in the H-Pol response as the orientation of the e-field reflects more readily off the ground plane. This is less visible in the V-Pol as the electric field wave variation is oriented orthogonal to the reflection plane, causing less phase summing deviation. The anechoic chamber should not produce reflections, however, due to the wooden floor above the lower RAM, reflections are produced. These reflections are reduced compared to the sports field, however, are still visible in the anechoic chamber H-Pol trace in Figure 4.1.

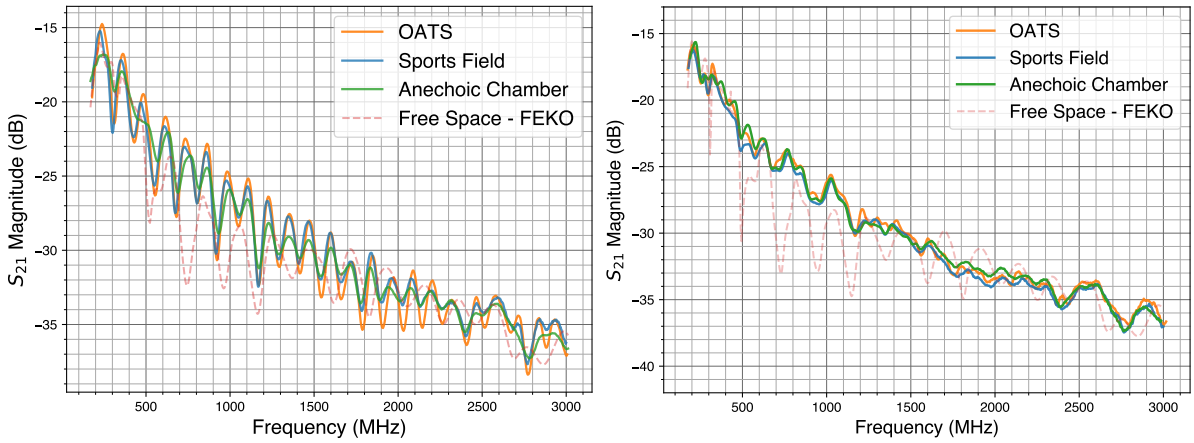

Figure 4.1: H-Pol and V-Pol S_{21} comparison between the OATS, sports field, anechoic chamber and FEKO - free space (R = 3 m).

An interesting addition to the plot is the FEKO free space response. The H-Pol and V-Pol are the same, as would be expected, in free space. The response shows the impedance mismatch across the frequency range has an impact on the simulated model. This is most likely caused due to the elements being modelled as wires. To ensure that this was not due to near-field issues, a simulation at R = 14 m was run with results showing similar transmission degradation in the 500 MHz to 1500 MHz range as seen in Figure 4.1's *Free Space - FEKO* trace.

4.3 Data Filtering

The Savitzky-Golay filter was created by Savitzky and Golay (1964). This digital filter can smooth data without distorting the tendency of the underlying data. The smoothing is achieved by fitting successive sub-sets of data with a low degree polynomial. Applying this filter with a 3rd order polynomial and a window size of 39 to the different responses achieved the results seen in Figure 4.2. It can be seen that by filtering the H-Pol response for the sports field and OATS, the reflections from the ground plane were removed. Forming a trace that correlates well with the V-Pol orientation of the anechoic chamber measurement.

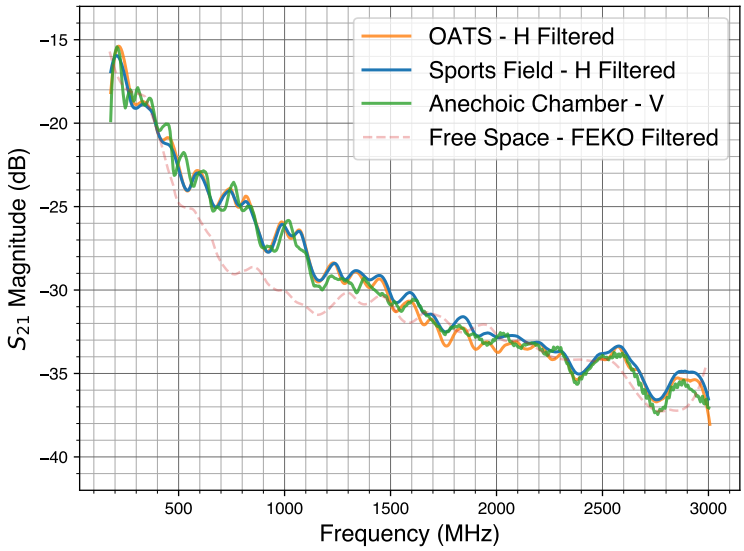

Figure 4.2: Coefficient of transmission at the OATS, FEKO and sports field's filtered H-pol. Compared with the anechoic chamber V-Pol response.

A boresight transmission response for both H-Pol and V-Pol should be identical in free space, due to the ground reflections, however, this is not the case. V-Pol gives the least influenced response from a ground plane, and therefore, this is used to compare to the filtered H-Pol results. Showing that with filtering, the effect of the ground reflections can be digitally removed.

This provides a major improvement on the conventional reflection range method suggested by Balanis (2016) where manually changing heights and calculating maximum and minimum values for each frequency is required. In a much shorter time-frame, with single measurements and digital filtering, accurate results can be obtained.

4.4 Antenna Gain

The gain response for the vertical and horizontal polarisation is shown in Figure 4.3 below. The plots show the filtered and unfiltered response to highlight the filtering effect. As the unfiltered

S_{21} values are used in calculating the gain, the oscillations are magnified. This highlights one factor for the sports field in that, as the E-field does not reflect off of the soil ground plane as effectively, the amount of variations are fewer, which in turn delivers a slightly smoother gain response. The disadvantage of this, however, is that the sports field permittivity is not uniform, making it difficult to de-embed the reflected wave from the direct wave. A metal ground plane, where the permittivity is constant, can be more accurately de-embedded.

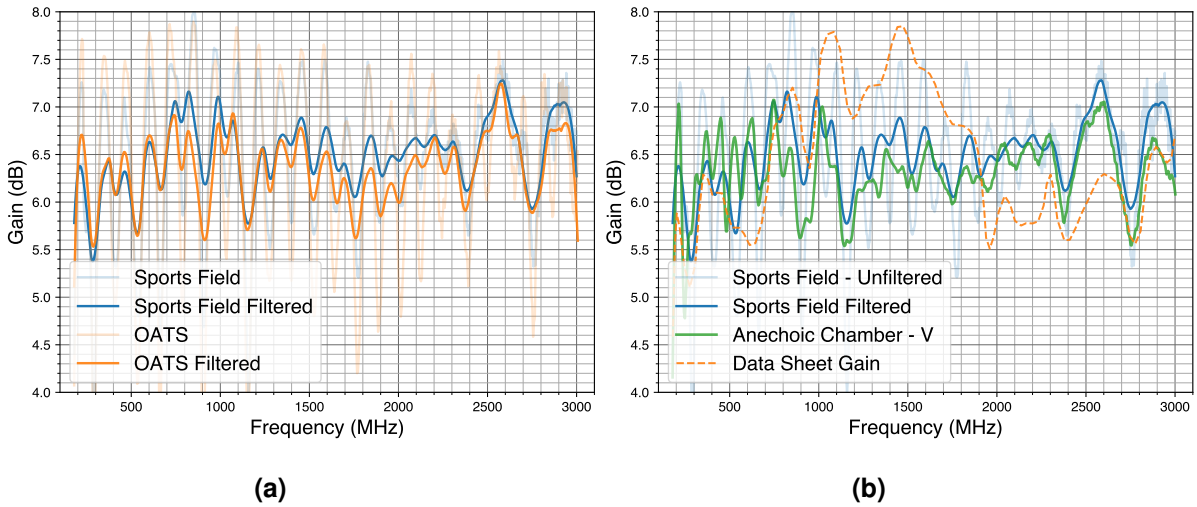

Figure 4.3: Boresight gain comparisons between: (a) The sports field and OATS, filtered and unfiltered (H-Pol); (b) Anechoic chamber V-Pol and the A-INFO (2018) specification sheet gain compared with the filtered sports field H-Pol measurement.

It is unknown exactly how the data sheet gain plot (dashed orange trace) was achieved, however, it varies from 5 dB at 180 MHz to 7 dB at 1000 MHz. It consists of two peak gain points of 7.78 dB and 7.85 dB at 1050 MHz and 1450 MHz respectively. The remainder of the trace drops down to 5.5 dB at 1950 MHz where it then ranges from this point to 6.7 dB gain at 3000 MHz.

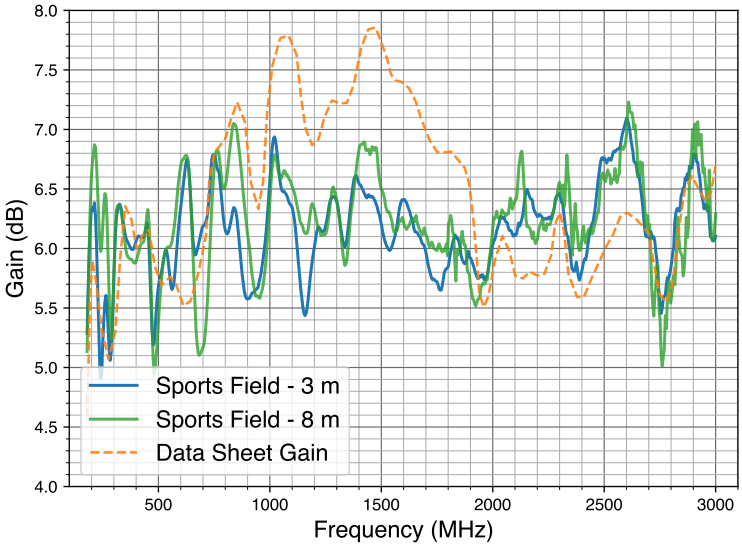

Figure 4.4: Measured gain for R = 3 m and R = 8 m on sports field (V-Pol), compared with the A-INFO (2018) specification sheet gain.

The actual measurements made oscillates far more frequently. However, this oscillation decreases between 1200 MHz and 2200 MHz. It was assumed that this might be due to not meeting the far field distance, yet Figure 4.4 shows the result where the separation distance is increased from 3 m to 8 m, and still there is no significant change.

There is more noise on the 8 m trace as the signal gets affected by the larger separation distance. This is caused by the device reaching the limit of its dynamic range, most prominent at higher frequencies. This signal, however, is still very similar to the R = 3 m trace and can be cleaned with the Savitzky-Golay filter to remove most of the high-frequency noise.

Table 4.1: Boresight gain at different frequencies for sports field and anechoic chamber. Difference = sports field gain - anechoic chamber gain. Also shown is the difference between sports field and data sheet gain as taken from A-INFO (2018).

Frequency (MHz)	Sports field (dB)	Anechoic chamber (dB)	Difference (dB)
200	6.36	6.65	-0.29
500	5.68	6.14	-0.46
1000	6.59	6.79	-0.2
1500	6.20	6.20	0
2000	6.03	6.43	-0.4
2500	6.76	6.83	-0.07
3000	6.13	6.25	-0.12
	Sports field (dB)	**Data sheet (dB)**	**Difference (dB)**
200	6.36	5.81	0.55
500	5.68	5.77	-0.09
1000	6.59	7.35	-0.76
1500	6.20	7.73	-1.53
2000	6.03	5.80	0.23
2500	6.76	5.98	0.78
3000	6.13	6.68	-0.55

Table 4.1 quantifies the difference between the gain achieved on the sports field compared to the anechoic chamber and the data sheet for seven different frequency points. Figure 4.5 shows the comparison plot between the gain measured on the sports field vs the anechoic chamber and data sheet. This plot is achieved by subtracting either gain from the sports field measured gain. Therefore, if the trace is positive, the gain measured on the sports field is more than the removed gain trace.

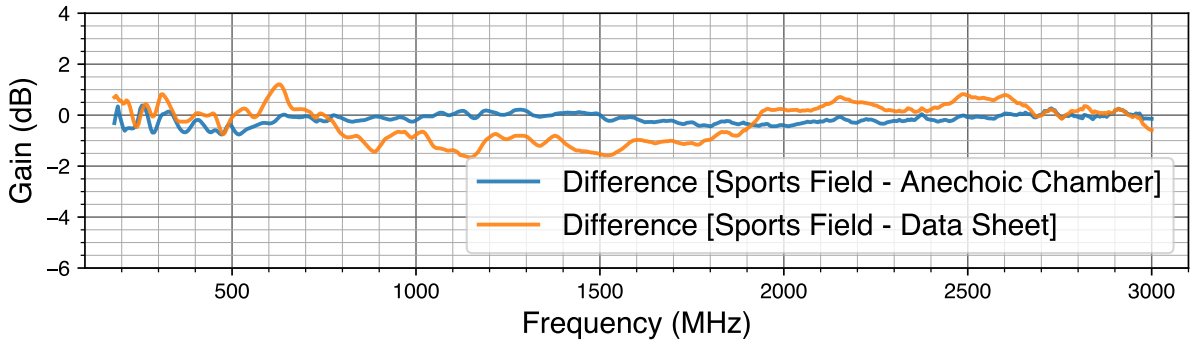

Figure 4.5: Boresight gain difference plot between the V-Pol sports field and anechoic chamber as well as data sheet.

The largest difference compared to the data sheet is -1.66 dB at 1150 MHz, while for the anechoic chamber the largest difference is 0.74 dB at 215 MHz. Of the seven different frequency points shown in Table 4.1, more than half are under 0.3 dB when comparing the sports field to the anechoic chamber. For the sports field versus data sheet, only 1 measurement point is above 0.8 dB. This shows that although one or two points are not as accurate, the majority of the boresight measurements taken on the sports field are within 1 dB of the data sheet, and even closer for the anechoic chamber measurement.

4.5 Gain Pattern

Figure 4.6 shows the difference between A-INFO (2018) data sheet, FEKO 3D far field request, OATS as well as the anechoic chamber and sports field measurements. These are shown here for 200 MHZ and 600 MHz (H-Pol). The 200 MHz plot indicates pattern similarities between the measured and data sheet patterns, however, the simulated free space 3D pattern follows the data sheet the best.

With reference to Figure 4.4 it is noted that at both 200 MHz and 600 MHz, there is a large difference between the measured and data sheet gain, this directly correlates to the difference in the boresight gain measured for these frequencies. The 90° nulls seen in the 200 MHz H-Pol are not as prominent in the measured results due to the limited rotation resolution of 5° and the small separation distance which does not allow for a planar wave-front to form as mentioned in Section 2.2.1.

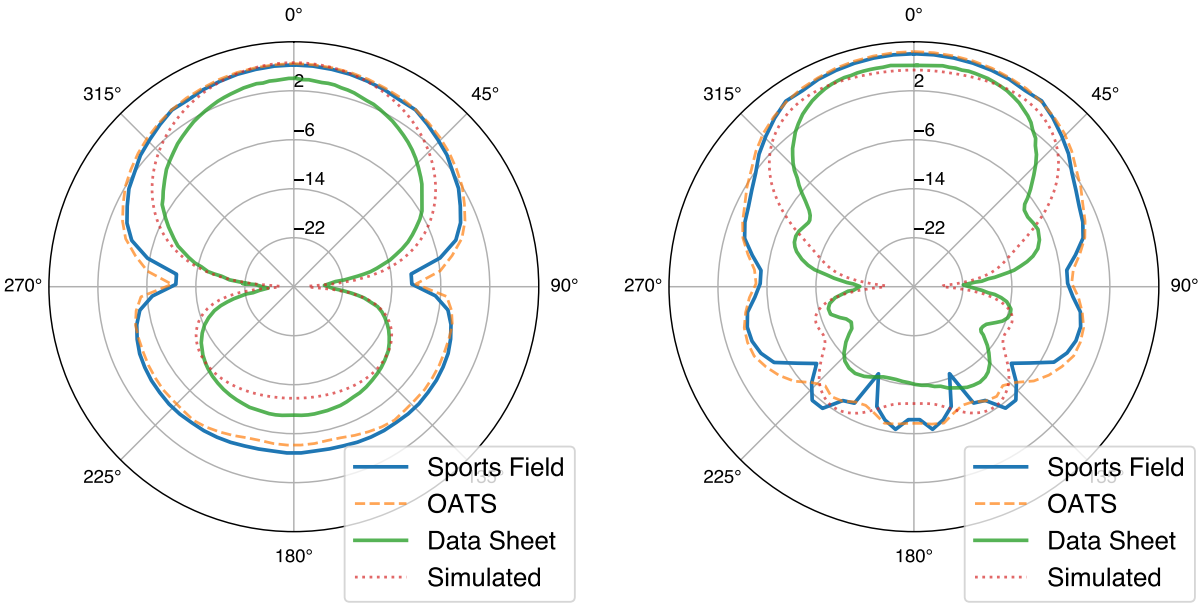

200 MHz H-Pol **600 MHz H-Pol**

Figure 4.6: Gain pattern comparisons between sports field and OATS measurements, compared to FEKO simulated and A-INFO LPDA specification sheet patterns taken from A-INFO (2018). Shown here for 200 and 600 MHz H-Pol.

A general theme for the polar plots is that the sports field results correlate well with the OATS and anechoic chamber measurements throughout Figures 4.6 and 4.7. The main lobe correlates well for the higher frequencies (larger than 1 GHz) . The frequencies used align with the available patterns presented in the data sheet. However, using the written *Polar Plot* code given in Appendix D.2 any frequency point measured can be plotted.

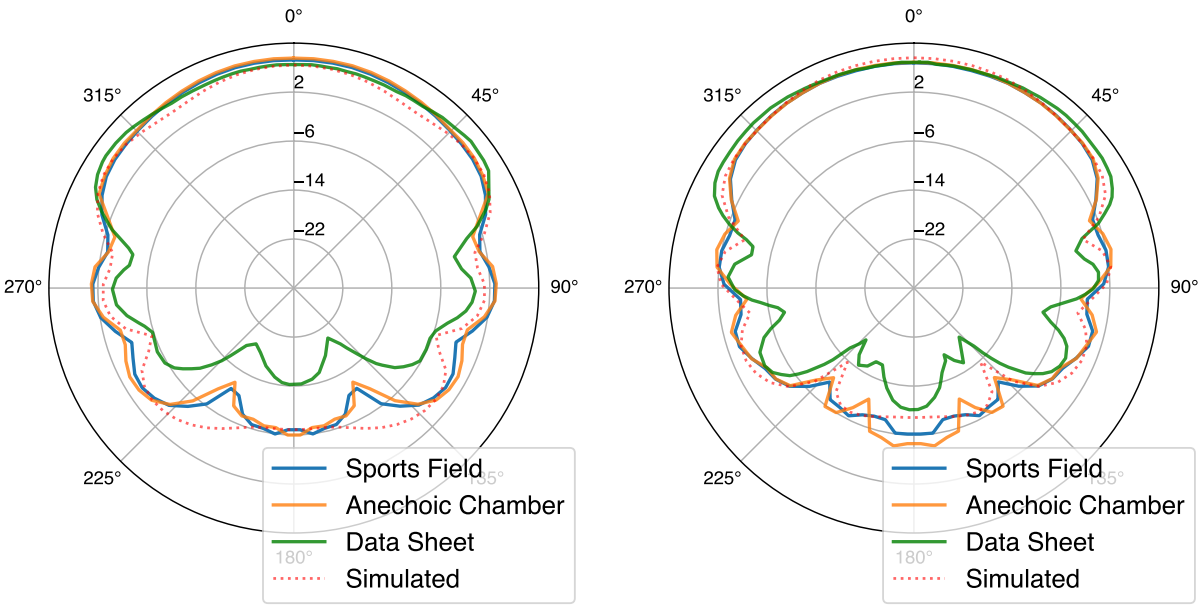

1 GHz V-Pol **1.5 GHz V-Pol**

Figure 4.7: Gain pattern for sports field and OATS measurements, compared to FEKO simulated and A-INFO LPDA specification sheet taken from A-INFO (2018), for 1 and 1.5 GHz V-Pol.

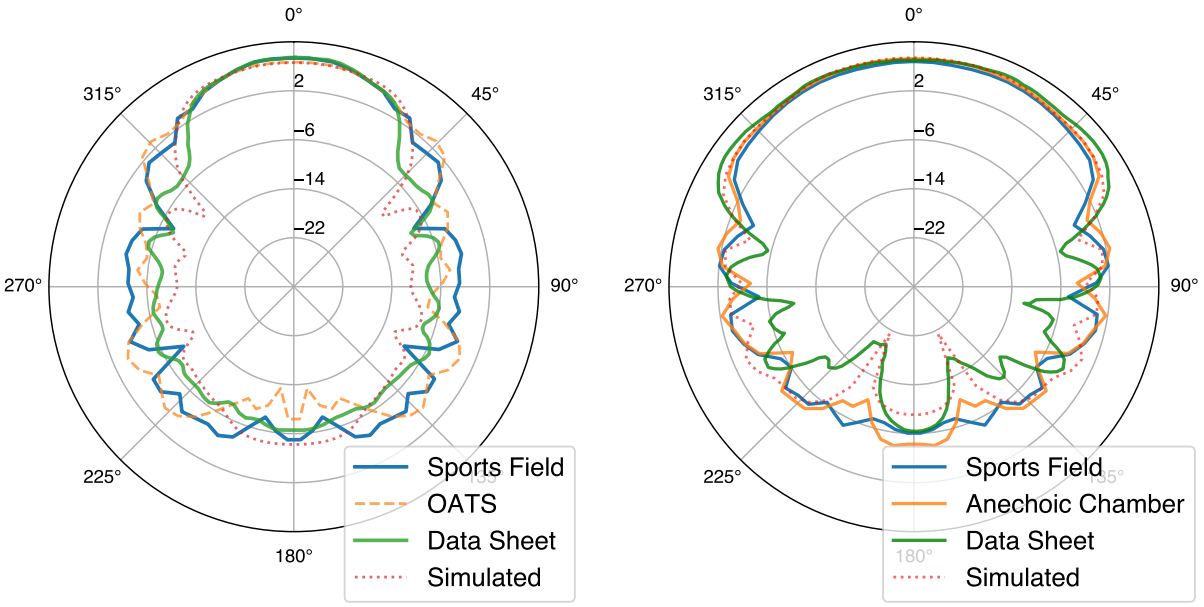

2 GHz H-Pol **2 GHz V-Pol**

Figure 4.8: Gain pattern for sports field and OATS measurements, compared to FEKO simulated and A-INFO LPDA specification sheet taken from A-INFO (2018), for 2 GHz H- and V-Pol.

Compared to the lower frequency plots in Figure 4.6, the higher frequencies correlate better to the data sheet as illustrated in Figure 4.7 and 4.8 . This improvement is attributed to the shorter wavelength of the higher frequencies which causes less transmission variation from the mean (see Figure 4.1).

Figure 4.9 below is meant to highlight the comparison for the H-Pol of the sports field and anechoic chamber. The V-Pol similarities can be seen in Figure 4.7 above.

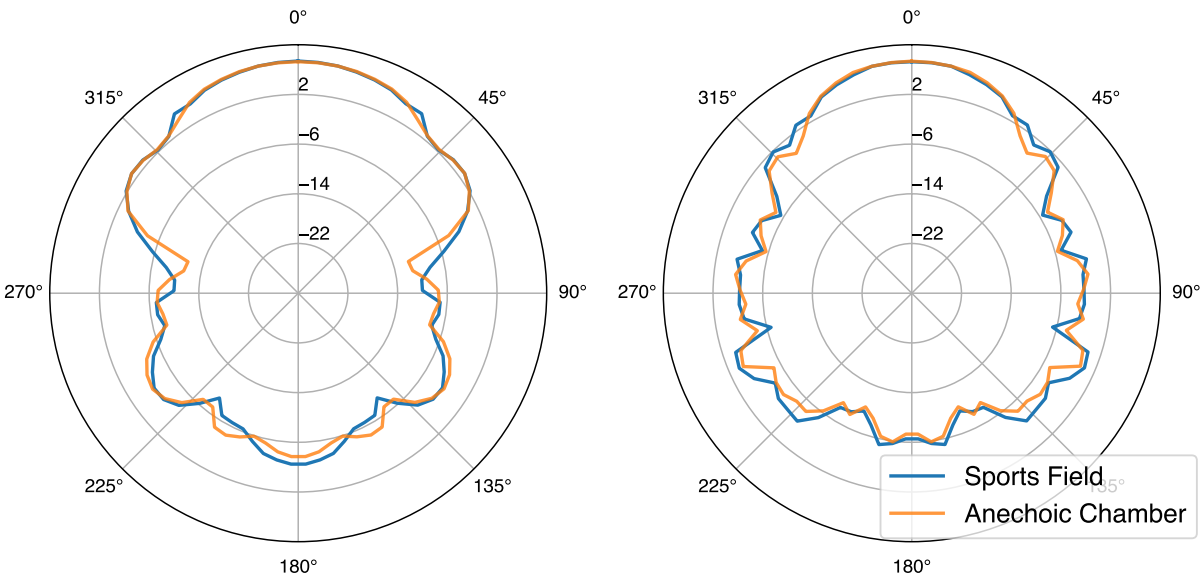

1 GHz H-Pol **2.5 GHz H-Pol**

Figure 4.9: Gain pattern comparisons between sports field and the anechoic chamber, for 1 and 2.5 GHz H-Pol.

The strong correlation between the sports field and anechoic chamber for both the V-Pol and H-Pol show promising results for using the sports field as an antenna measurement range. The measurement accuracy will be quantified in the next section.

4.6 Measurement Result Comparison

Table 4.2 was produced for 1 and 2 GHz vertical polarized patterns, this polarization was chosen as it is not as affected by the ground plane. The 1 GHz and 2 GHz frequencies were used as the patterns have complex shapes and give 500 MHz variation near the centre frequency of UHF. The background spectrum measurement (Figure 3.22) is also quite for these frequencies.

This table shows the level of accuracy that could be expected from a sports field measurement compared to the data sheet. It should be noted, however, that the data sheet polar patterns were from a batch antenna measurement made in 2014, when the antenna was manufactured.

Table 4.2: Polar pattern difference for 1 GHz and 2 GHz V-Pol (sports field vs data sheet).

Freq. = 1 GHz	**Sports field (dB)**	**Data sheet (dB)**	**Difference (dB)**
$0°$	7.3	6.4	0.9
$45°$	6.2	7.1	0.9
$90°$	2.7	-0.5	3.2
$135°$	-2.9	-14	11.1
$180°$	-6.9	-14.2	7.3
Freq. = 2 GHz			
$0°$	6.7	6.9	0.2
$45°$	5.8	7.4	1.6
$90°$	-1.8	-0.3	1.5
$135°$	-4.2	-9.2	5
$180°$	-6	-6.4	0.4

Due to the uncertainties in the antenna data sheet, an alternative comparison would be between the sports field and the anechoic chamber measurements. This is a direct comparison between the same antennas and measurement equipment with the only variable being the test facility.

Table 4.3: Polar pattern difference for 1 GHz and 2 GHz V-Pol (sports field vs anechoic chamber).

Freq. = 1 GHz	Sports field (dB)	Anechoic Chamber (dB)	Difference (dB)
$0°$	7.3	7.7	0.4
$45°$	6.2	6.2	0
$90°$	2.7	2.8	0.1
$135°$	-2.9	-3.4	0.5
$180°$	-6.9	-6.1	0.8
Freq. = 2 GHz			
$0°$	6.7	7.3	0.6
$45°$	5.8	6.4	0.6
$90°$	-1.8	-2.6	0.8
$135°$	-4.2	-3.2	1
$180°$	-6	-4.3	1.7

Figures 4.7 and 4.9 show the comparison for V-Pol and H-Pol respectively. Table 4.3 shows that the V-Pol measurements for the anechoic chamber and sports field gain patterns correlate to within 2 dB with the biggest difference (1.7 dB) at the back lobe for 2 GHz.

4.7 Measurement Costing

The cost associated with the measurements made have been outlined in the Table 4.4 below.

Table 4.4: Equipment cost to achieve sports field measurements.

Equipment	Description	Type	Approx. Cost (R)
Coaxial Cable	N-Type male cables, 2 x 5 m	Cables	6,000
NanoVNA V2	Transmission reflection, 2-port, 50 kHz - 3.6 GHz	VNA	1,200
PVC Piping	50 mm PVC pipe, available at hardware store, 9 m/tripod	Pipe	600
3D Prints	Antenna Mounts and connector blocks	Mounts	500
Connectors	N-Type to SMA	connectors	600
Consumables	Duct tape, plastic screws, rope/string		250
		TOTAL	9,150

For R9,150 antenna measurements can be made on a sports field to within a few dB. This cost is orders of magnitude less than the commercial equipment outlined in Table 3.1. The costing does not include a computer/laptop as most students and engineers have this available.

4.8 Conclusion

Measurements made on the sports field are comparable to the data sheet and anechoic chamber results. The boresight measurements correlate particularly well with the anechoic chamber, achieving similarities to within 0.74 dB for gain measurements. The data sheets gain has a larger maximum difference of 1.66 dB compared to the sports field gain results. Using the Savitzky-Golay filter allowed for majority removal of the ground reflections from horizontal measurements as shown in Figure 4.3, improving the achievable accuracy for boresight measurements.

The measured gain patterns showed similar shapes to the data sheet, however, the measured results did not show deep nulls, most likely due to the short separation distance which does not allow a planar wave-front to form. The largest pattern difference was seen at the lower frequencies (Figure 4.6) where the reflection of the longer wavelengths causes more variation. Frequencies from 1 GHz showed main lobe agreement to within 1 dB with larger variance for the rear lobes compared to the data sheet. Having compared and discussed the results from all the measurements, the next section will cover recommendations and insights obtained along the way.

Chapter 5

Conclusion and Recommendations

Due to the wide use of antennas and the ever-growing interest in wireless control, the ability to experiment with and measure antennas at tertiary education institutions is paramount. The cost to implement a dedicated test facility is, however, often prohibitive. For these reasons, research was conducted to highlight the ability of using cost-effective VNAs, tripods and available facilities to answer the following questions:

What methods and equipment can be used to accurately and cost-effectively characterise antennas on a sports field?

By using a NanoRFE (2019) NanoVNA, PVC piping and a 3D printed parts, the two antenna method can be implemented on a sports field to make boresight gain and gain pattern measurements as discussed in Chapter 4.

How does a sports field response compare to dedicated antenna testing ranges?

Using the two antenna method on the sports field, boresight gain results were achieved to within 1.66 dB of the data sheet when vertically polarized. The H-Pol is not as accurate due to the electric fields reflecting off the ground plane to produce multi-path reflections seen in Figure 4.1. These reflections can be removed by using a Savitzky-Golay filter to smooth the data without changing the underlying tendencies of the data as illustrated in Figure 4.3 (b). Using the Savitzky-Golay filter, the boresight gain measurements between the anechoic chamber and sports field differed by less than 0.74 dB as seen in Figure 4.5. The filter allows simplification and decreases measurement time compared to the ground reflection method discussed in Section 2.6.5, removing the need to change antenna heights for each frequency of interest.

To what level of accuracy can an unknown antenna be characterised on a sports field?

The research achieved boresight gain results on a sports field to accuracies within 0.74 dB for V-Pol and 1.75 dB (unfiltered) for H-Pol compared to a dedicated anechoic chamber. The available data sheet showed larger variation as seen in Figure 4.4, however, the results for this are still within 1.55 dB accuracy. The Polar patterns show agreement within 3 dB for sports field vs anechoic chamber. The data sheet has more differences compared to the measured data as outlined in Table 4.1, with the largest being 11.1 dB at 135° for 1 GHz. The 0 - 45° (main

lobe) agrees to within 0.5 dB for the same measurement.

This research has shown that for a fraction of the cost, and by using a sports field as an antenna test range, satisfactory results can be achieved in the UHF band. This allows students to accurately test antennas for under R10,000 where as before, a dedicated test facility, costing R10,000 to rent per day, was advised.

5.1 Recommendations

To assist with successful measurements, below is a list of recommendations and practical tips to consider when planning antenna measurements.

- Booking of the sports field is essential to ensure that the irrigation is turned off and that no sports matches/practice will interfere with measurements.
- Electrical power, if required, is usually only available at the peripheries of the field, therefore, a long power extension may be required.
- When setting up the antennas take into account any metal signboards, stadiums or features that could produce unwanted reflections. If doing a polar pattern measurement take this into account for the antenna rotation.
- The flat, open area leaves one exposed to the elements, a weather check several days in advance is advised. Wind can cause measurement difficulties, however, due to the design of the tripod it allows the legs to be filled with sand. This adds weight to ensure the tripods and antenna do not blow over.
- Horizontally polarized measurements are affected by the ground reflections. This could be digitally filtered or mitigated in measurement by using radar absorbing material at the reflection point between the two antennas.
- A background spectrum measurement is advised as sports fields at other locations may be in a RF noisy environment. This also allows one to be cognisant of background features, if present in measurements.
- The NanoVNA is battery powered, however, without a computer it can only log 201 points. For more measurement points a battery powered laptop is advised as the nearest plug is 50 m away.

Although measurements usually take longer than anticipated, an indoor test run will ensure successful measurement planning has been achieved.

Bibliography

A-INFO, C. 2018. “A - Info DS-18300 Technical Specifications.” https://www.bbrc.ru/upload/iblock/a98/5ca2b850_e6a4_11ea_80de_0cc47a1243ef_f363d9a1_e6a4_11ea_80de_0cc47a1243ef.pdf. [Accessed: 20.05.2020].

Adhyapak, A., Z. Chen and K. Shimada. 2017. Free space antenna factor computation using time domain gating and deconvolution filter for site validation of fully anechoic rooms. In *2017 IEEE International Symposium on Electromagnetic Compatibility & Signal/Power Integrity (EMCSI)*. IEEE pp. 486–491.

Altair FEKO. 2021. “Altair Simulation Products.” www.altair.com. [Accessed: 10.01.2021].

Ambatali, Charleston Dale M. 2018. Implementation of an oscilloscope vector network analyzer for teaching s-parameter measurements. In *2018 IEEE Region 10 Humanitarian Technology Conference (R10-HTC)*. IEEE pp. 1–6.

Ameya, Michitaka, Sayaka Matsukawa and Satoru Kurokawa. 2018. Antenna gain self-calibration method with moving flat reflector for millimeter-wave frequency band. In *2018 IEEE Conference on Antenna Measurements & Applications (CAMA)*. IEEE pp. 1–4.

Arnold, P. 1966. “The “Slant” antenna range.” *IEEE Transactions on Antennas and Propagation* 14(5):pp.658–659.

Balanis, C.A. 2016. *Antenna Theory : Analysis and Design*. 4th ed. United States of America: John Wiley & Sons Inc.

Bevelacqua, P. 2015. “Antenna-Theory.com!” https://www.antenna-theory.com/. [Accessed: 21.04.2021].

Chen, G., J. Stang and M. Moghaddam. 2016. “A conformal FDTD method with accurate waveport excitation and S-parameter extraction.” *IEEE Transactions on Antennas and Propagation* 64(10):pp.4504–4509.

Chen, Z. and Z. Xiong. 2019. Mitigation of band edge effects in fourier transform based time domain gating. In *2019 13th European Conference on Antennas and Propagation (EuCAP)*. IEEE pp. 1–5.

Connor, F.R. 1983. *Antennas. Introductory topics in electronics and telecommunication*, London: Edward Arnold.

DuHamel, R. and D Isbell. 1957. Broadband logarithmically periodic antenna structures. In *1958 IRE International Convention Record*. Vol. 5 IEEE pp. 119–128.

Dunsmore, J. 2007. “Network Analyzer Basics- EE142 Fall 07.” http://rfic.eecs.berkeley.edu/142/pdf/NABasicsNotes.pdf.

Edy555. 2019. “About NanoVNA.” https://nanovna.com/. [Accessed: 30.04.2020].

Evans, G.E. 1990. *Antenna Measurement Techniques*. London: Artech House Publishers.

Foegelle, Michael D. 2002. “Antenna pattern measurement: concepts and techniques.” *Compliance Engineering* 19(3):22–33.

Fordham, Jeffrey A. 2016. “An introduction to antenna test ranges, measurements and instrumentation.” *Microwave Instrumentation Technologies, LLC* .

Friis, Harald T. 1946. “A note on a simple transmission formula.” *Proceedings of the IRE* 34(5):254–256.

Fukasawa, T., T. Yanagi, H. Miyashita and Y. Konishi. 2012. "Extended S-parameter method including radiation pattern measurements of an antenna." *IEEE Transactions on antennas and propagation* 60(12):pp.5645–5653.

Gilmour, A.S. 1986. *Microwave Tubes.* Artech House microwave library Artech House.

Glimm, J, K Münter, R Pape and M Spitzer. 2000. New results of antenna-calibration in a single-antenna set-up. In *XVI IMEKO World Congress*. pp. 25–28.

Hemming, L. and R. Heaton. 1973. "Antenna gain calibration on a ground reflection range." *IEEE Transactions on Antennas and Propagation* 21(4):pp. 532–538.

Hiebel, M. 2007. *Fundamentals of Vector Network Analysis*. Germany: Rohde & Schwarz GmbH & Co. KG.

International Telecommunication Union, ITU-R. 2021. "Rec. ITU-R P.527-6: Electrical characteristics of the surface of the Earth." https://www.itu.int/dms_pubrec/itu-r/rec/p/R-REC-P.527-6-202109-I!!PDF-E.pdf. [Accessed: 20.11.2021].

Isbell, D. 1960. "Log periodic dipole arrays." *IRE transactions on antennas and propagation* 8(3):260–267.

John, A. 2021. "1 to 4 GHz: nanoVNA 2 Plus4 vs. Keysight FieldFox." https://ae5x.blogspot.com/2021/07/1-to-4-ghz-nanovna-2-plus4-vs-keysight.html. [Accessed: 01.09.2021].

Julies, T.G. 2018. Time-domain Antenna Characterization. Master's thesis Stellenbosch: Stellenbosch University.

Kibona, Lusekelo. 2013. "Gain and directivity analysis of the log periodic antenna." *International Journal of Scientific Engineering and Research (IJSER)* 1(3):14–18.

Koech, J.C. 2019. Modified horn-type antennas for SKA RFI Monitoring. Master's thesis Stellenbosch: Stellenbosch University.

Kriel, Scott GH and Dirk IL de Villiers. 2020. "Mutual Coupling Effects Between Test and Reference Antennas in Near-Field Measurements." *URSI RADIO SCIENCE LETTERS* 2.

Mistry, K.K., P.I. Lazaridis, Z.D. Zaharis, M. Akinsolu, B. Liu and T. Loh. 2019. "Accurate antenna gain estimation using the two-antenna method." *in IET Conference Proceedings* .

NanoRFE, H. 2019. "About NanoVNA V2." https://nanorfe.com/nanovna-v2.html. [Accessed: 28.04.2020].

Nyikayaramba, Gift and Boris Murmann. 2020. "S-Parameter-Based Defect Localization for Ultrasonic Guided Wave SHM." *Aerospace* 7(3):33.

OwOComm. 2020. "S-A-A-2 User Guide." https://nanorfe.com/nanovna-v2.html. [Accessed: 28.04.2020].

Phiri, T.J. 2017. Characterising the electromagnetic environment of MeerKAT. PhD thesis Stellenbosch: Stellenbosch University.

Sandrawarman, A. 2014. Antenna Gain Measurement Using Image Theory. PhD thesis Universiti Tun Hussein Onn Malaysia.

Savitzky, Abraham and Marcel JE Golay. 1964. "Smoothing and differentiation of data by simplified least squares procedures." *Analytical chemistry* 36(8):1627–1639.

TechAmerica. 2009. "Touchstone® File Format Specification." http://www.ibis.org/touchstone_ver2.0/touchstone_ver2_0.pdf. [Accessed: 20.05.2021].

What is dBi - Antenna Gain. 2021. https://www.everythingrf.com/community/what-is-dbi. Accessed: 2021-04-28.

Yanagi, T., T. Fukasawa and H. Miyashita. 2016. "Extended S-Parameter Method for Measuring Reflection and Mutual Coupling of Multi-Antennas." *IEICE Transactions on Communications* 99(10):pp.2195–2202.

A P P E N D I C E S

Appendix A

NanoVNA Specifications

Parameter	Board version	Specification	Conditions
Frequency range	V2_2, V2 Plus	50kHz - 3GHz	-
	V2 Plus4, V2 Plus4 Pro	**50kHz – 4.4GHz**	-
Frequency resolution	All	0.01MHz	-
System dynamic range (calibrated)	V2_2, V2 Plus	70dB	1GHz
		60dB	3GHz
	V2 Plus4	**90dB**	**1GHz BW=6.2kHz, AVG=20**
		80dB	**3GHz BW=6.2kHz, AVG=5**
	V2 Plus4 Pro	**90dB**	**1GHz BW=1.6kHz, AVG=5**
		80dB	**3GHz BW=1.6kHz, NO AVG**
S11 noise floor (calibrated)	All	-50dB	f < 1.5GHz
		-40dB	f < 3GHz
Sweep points	V2 Plus4	1 – 1024 points (with NanoVNA-QT software). More points (up to 65535) are possible depending on the performance of your PC.	-
Sweep time	V2 Plus4	0.25s	Default sweep settings
	V2 Plus4 Pro	0.16s	Default sweep settings BW=10kHz
Power supply	All	USB, 4.6V – 5.5V	-
Supply current	All	500mA typ	No charging
Battery current, charging	All	1.2A typ	-
Battery capacity	V2 Plus4, V2 Plus4 Pro	3200mAh	-
Operation ambient temperature	All	0°C - 45°C *	* by design, not tested in production
Ambient temperature during battery charging	All	10°C - 45°C	-

Figure A.1: NanoVNA specifications taken from NanoRFE (2019)

Appendix B

FEKO 3D Far-Field Pattern

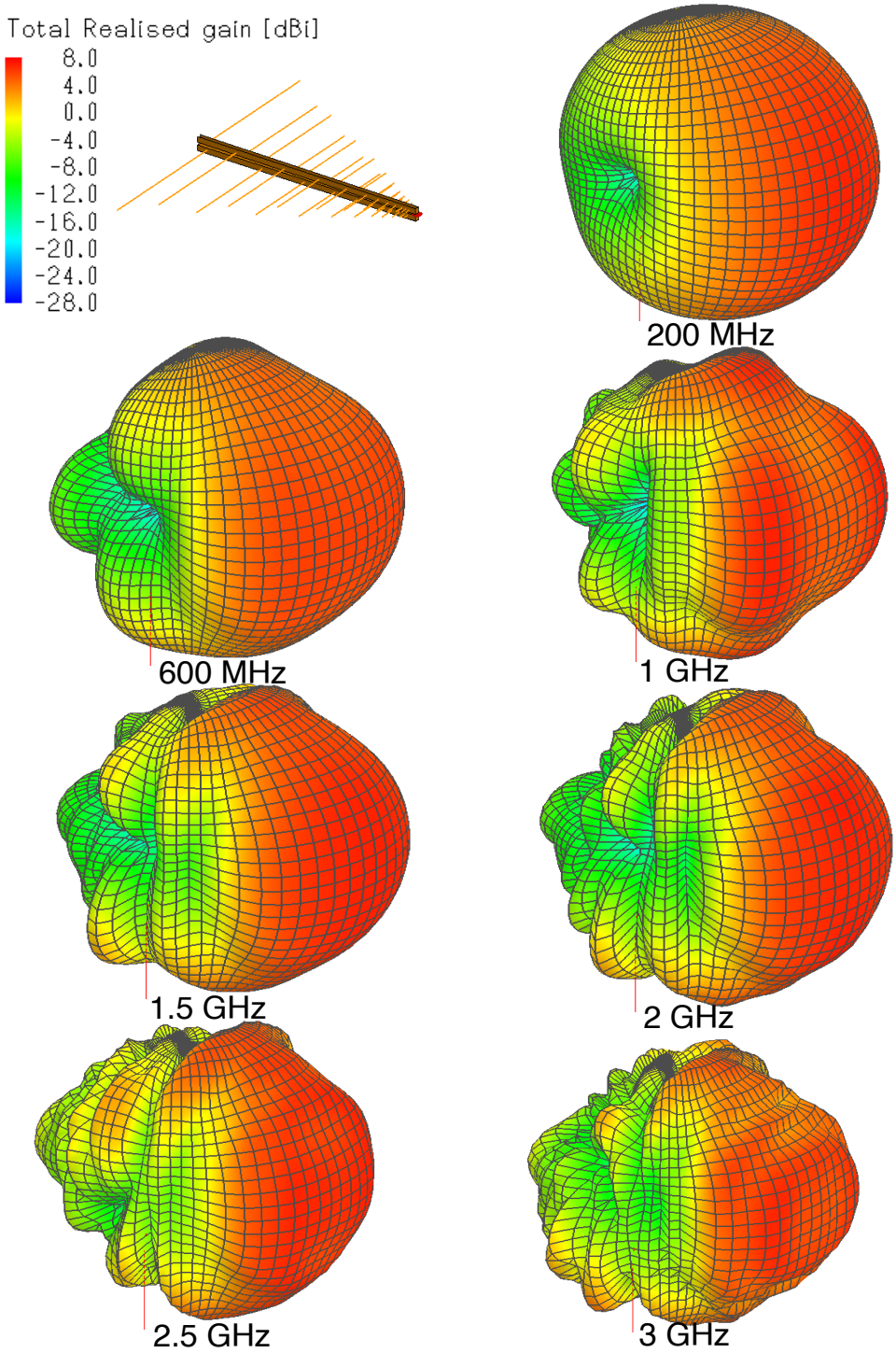

Figure B.1: A-INFO LPDA 3D polar pattern for various frequencies as simulated in Altair FEKO (2021).

Appendix C

Far-Field vs Near-Field FEKO Plot

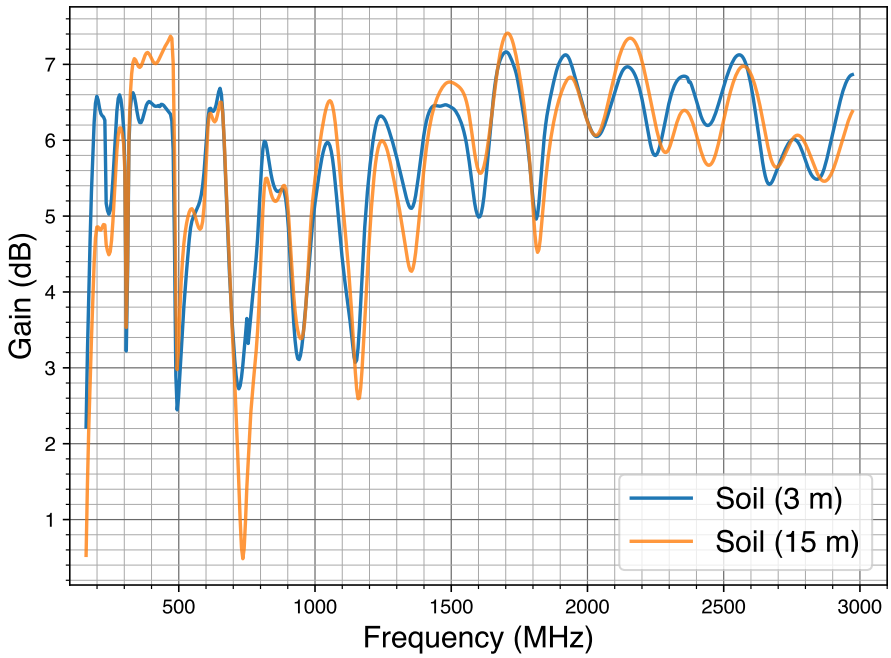

Figure C.1: FEKO gain comparison between R = 15 and R = 3 m for V-Pol

Appendix D

Python Code

D.1 Multiple .snp Files to .xlsx File

The code below converts the 37 angle files into one .xlsx document for processing. Each angle is placed on a separate sheet.

```
#By Casey Bryant 2021
#Used to prepare 37 different angled files for polar plotting
#Convert multiple NanoVNA .s2p files to one, multi sheet XLSX file.

import pandas as pd
filename = 'Combined 3mh.xlsx' #Output file name

files=('0deg.s2p','5deg.s2p','10deg.s2p','15deg.s2p','20deg.s2p','25deg.s2p',
'30deg.s2p', '35deg.s2p', '40deg.s2p', '45deg.s2p', '50deg.s2p', '55deg.s2p',
'60deg.s2p', '65deg.s2p', '70deg.s2p', '75deg.s2p', '80deg.s2p', '85deg.s2p',
'90deg.s2p', '95deg.s2p', '100deg.s2p', '105deg.s2p', '110deg.s2p',
'115deg.s2p','120deg.s2p', '125deg.s2p', '130deg.s2p', '135deg.s2p',
'140deg.s2p', '145deg.s2p', '150deg.s2p', '155deg.s2p', '160deg.s2p',
'165deg.s2p', '170deg.s2p', '175deg.s2p', '180deg.s2p')

writer = pd.ExcelWriter(filename) #Create file

for file in files: #for loop to run through files listed above
  with open(file) as f:

lines = f.readlines()[11:]               # read the data from row 11
   F = [float(line.split()[0]) for line in lines] #Column 0 holds frequency
S_11 = [float(line.split()[1]) for line in lines] #Column 1 holds $S_{11}$
S_21 = [float(line.split()[3]) for line in lines] #Column 3 holds $S_{21}$
S_12 = [float(line.split()[5]) for line in lines] #Column 5 holds $S_{12}$
S_22 = [float(line.split()[7]) for line in lines] #Column 7 holds $S_{22}$

Freq = pd.DataFrame (F) #Take split data and put into a dataframe
S11 = pd.DataFrame (S_11)
S21 = pd.DataFrame (S_21)
S12 = pd.DataFrame (S_12)
S22 = pd.DataFrame (S_22)
```

```
data = pd.concat([Freq, S11, S21, S12, S22], axis = 1) # concatenate the
                                        dataframe
data.columns = ['Frequency (Hz)', 'S11', 'S21', 'S12', 'S22'] #heading labels

data.to_excel(writer, sheet_name = '%s' % file, index=False) #write data to
                                        file.
writer.save()
print ('Writer saved as %s' % filename)
```

D.2 Python Polar Plot Code

The following code uses the output .xlsx file from the code above. It will plot the gain pattern for the *rowP* frequency set in the variables section of the code.

```
############################################################
# Takes multi-sheet .XLSX file and creates a polar plot    #
# Created Date: 09/2021                                    #
# Author: Mr. Bryant C.J.N.M                               #
# Contact: bryant.casey1@gmail.com                         #
# Revision date 05/2022                                    #
############################################################
############################################################
#          ENSURE INPUT VARIABLES ARE CORRECT              #
############################################################

import openpyxl
import math as m
import pandas as pd
import matplotlib.pyplot as plt
import numpy as np

##########CONSTANTS#############

c = 299792458 #m/s Speed of light


###################VARIABLES################
file_name = 'Combined 3mh.xlsx'   # Set file name from previous code
orig = ('%s' % file_name)        # Original file to edit
new = ('Nov_3m_H.xlsx')          # New filename
R = 3                       # Distance between antennas
rowS = 2                    # Data Starting row
rowF = 1026                 # Data final row
rowP = 100                  # Row number to use for polar plot
```

```
############SELECT WORKBOOK################
print('Loading Workbook.....')
wb = openpyxl.load_workbook(orig)
print('Workbook Loaded!!!!!!')


############CLEAN WORKSHEET COLS############
print('Deleting extra column.....')
for col in wb.worksheets:
  col.delete_cols(7, 2)
  col.delete_cols(2, 4)


print('Creating Wavelength & Gain columns......')
for col_head in wb.worksheets:
  col_head['E1'] = 'Wavelength (m)'
  col_head['F1'] = 'Gain linear'
  col_head['G1'] = 'Gain (dB)'
  #col_head[''] = ''


##########Wavelength calc###########
print('Calculating wavelength.......')
for ws in wb.worksheets:
  for i in range(rowS, rowF):
  Freq = ws.cell(row=i, column=1).value
  Wl = c/Freq
  ws.cell(row=i, column=5).value = Wl
print('Wavelengths calculated!!!!!')

print('Calculating gains sheet..........')
for ws in wb.worksheets:
  for i in range(rowS, rowF): # rowS = start row, rowF = final row
    LMag = ws.cell(row=i, column=2).value
    Wl = ws.cell(row=i, column=5).value

#Formula below:
   FSPL =20*m.log10((4*3.14*r)/Wl)
   G = 0.5*(FSPL + 20*m.log10(LMag))
   ws.cell(row=i, column=6).value = FSPL #store FSPL into column 6
   ws.cell(row=i, column=7).value = G  #store G (Gain)  into column 6
print('Gains calculated!!!!!!!!')


###############SAVE NEW WORKSHEET##########
print('Saving workbook as %s...' % new)
```

```
 wb.save('%s' % new)
print('Workbook saved!!!!!')


df_new = pd.read_excel('%s' % new , '0deg.s2p')
print('Plotting Frequency vs Gain....')

df_Ainfo = pd.read_excel('C:/Users/Casey/Documents/To Do/Thesis/Results/A-Info
                                        Antenna/A-Info_Gain_Data.xlsx')
print('Plotting Frequency vs Gain A-Info....')


x = list(df_new['Frequency (Hz)'])
y = list(df_new['Gain (dB)'])

FreqA = list(df_Ainfo['Frequency (HzA)'])
GainA = list(df_Ainfo['Gain (dBA)'])



plt.figure(figsize = (15, 12))
plt.plot(x, y)
plt.plot(FreqA, GainA)
print('DONE!!!!!!')
plt.title('Gain for sheet 1')
plt.grid(True)

Gains1 = []
Gains2 = []

print('Loading Workbook.....')
wb = openpyxl.load_workbook('%s' % new)
print('Workbook Loaded!!!!!!')


for ws in wb.worksheets:
  G = ws.cell(row=rowP, column=7).value
  Gains1.append(G)
  Gains2.append(G)
#print(G)


Gains1.reverse()

Gains = Gains2 + Gains1
print(Gains)
```

```
X = max(Gains)
print(X)
print("max value")
sizeg = len(Gains)
print(sizeg)

deg = np.arange(0, 365, (365/74))
rads = (deg*3.14/180)

n = len(Gains)
x2 = np.arange(n)

sizer = len(rads)
print(sizer)

# Polar plot Setup
fig, ax = plt.subplots(subplot_kw={'projection': 'polar'})
ax.plot(rads, Gains)
ax.set_rmin(-30)
ax.set_rmax(10)
ax.set_rticks([-22, -14, -6, 2])# Less radial ticks
ax.set_rlabel_position(0)  # Move radial labels away from plotted line
ax.grid(True)
ax.set_theta_zero_location("N")  # theta=0 at the top
ax.set_theta_direction(-1)  # theta increasing clockwise
ax.set_title("1 GHz H-Plane 3m V2", va='bottom')
plt.show()
```